INFORMATION TO USERS

This manuscript has been reproduced from the microfilm master. UMI films the text directly from the original or copy submitted. Thus, some thesis and dissertation copies are in typewriter face, while others may be from any type of computer printer.

The quality of this reproduction is dependent upon the quality of the copy submitted. Broken or indistinct print, colored or poor quality illustrations and photographs, print bleedthrough, substandard margins, and improper alignment can adversely affect reproduction.

In the unlikely event that the author did not send UMI a complete manuscript and there are missing pages, these will be noted. Also, if unauthorized copyright material had to be removed, a note will indicate the deletion.

Oversize materials (e.g., maps, drawings, charts) are reproduced by sectioning the original, beginning at the upper left-hand corner and continuing from left to right in equal sections with small overlaps. Each original is also photographed in one exposure and is included in reduced form at the back of the book.

Photographs included in the original manuscript have been reproduced xerographically in this copy. Higher quality 6" x 9" black and white photographic prints are available for any photographs or illustrations appearing in this copy for an additional charge. Contact UMI directly to order.

UMI

A Bell & Howell Information Company
300 North Zeeb Road, Ann Arbor MI 48106-1346 USA
313/761-4700 800/521-0600

RICE UNIVERSITY

ABSOLUTE DIFFERENTIAL AND INTEGRAL CROSS SECTIONS FOR CHARGE TRANSFER OF STATE-SELECTED KEV O^+ WITH O_2

by

Robert L. Merrill

A THESIS SUBMITTED
IN PARTIAL FULFILLMENT OF THE
REQUIREMENTS FOR THE DEGREE

MASTER OF ARTS

APPROVED, THESIS COMMITTEE:

K. A. Smith
Distinguished Faculty Fellow, Physics
and Space Physics and Astronomy

Q. Si
Assistant Professor of Physics

J. P. Hannon
Professor of Physics

Houston, Texas
February, 1998

Abstract

Absolute Differential and Integral Cross Sections for Charge Transfer of State-selected keV O^+ with O_2

by

Robert L. Merrill

Absolute differential and integral charge transfer cross sections have been measured for 0.5, 0.85, 1.5, 2.8, and 5.0 keV O^+ with O_2 at scattering angles between 0.01^o and 3.50^o in the laboratory frame. The dependence of these cross sections upon the electronic state of the O^+ ion was investigated. This study was performed using a filter cell technique to derive the cross sections for both the $O^+(^4S)$ ground state ions and the $O^+(^2D, ^2P)$ metastable state ions. The charge transfer cross sections involving the $O^+(^2D, ^2P)$ ions are significantly larger than the corresponding cross sections for the ground state ions. Previously published cross section measurements are compared to the present results for the total integral charge transfer cross sections of state-selected keV O^+ with O_2.

Acknowledgments

I would like to thank my advisor Dr. Ken Smith and also Dr. Ronald Stebbings for their guidance. Also I would like to thank Drs. Bernard Lindsay and Chip Straub for their knowledge and assistance in the lab. Finally I would like to thank my wife Gretchen for her patience and support. I would also like to acknowledge the financial support given by the National Science Foundation, the National Aeronautics and Space Administration, and the Robert A. Welch Foundation.

Table of Contents

1. Introduction 1

2. Experimental Method and Apparatus
   - A. Charge Transfer Differential Cross Section Formula 3
   - B. Basic Overview 5
   - C. State Selective Analysis of the Primary Beam 14
   - D. Experimental Uncertainties 28

3. Results and Discussion
   - A. Differential Cross Sections 31
   - B. Integrals and Total Cross Sections 37

4. Conclusions and Recommendations 43

References 46

1. Introduction

Charge transfer differential cross sections of atomic oxygen ions with relevant atmospheric gases are of importance to atmospheric modelers, and they are of fundamental interest to physics. Significant fluxes of energetic O^+ ions with energies in the keV range have been observed by satellites to penetrate into the F-region of the Earth's atmosphere during geomagnetic storms[1]. These fast ions are readily neutralized by charge transfer reactions with O_2 and N_2, which are the two most abundant gases after atomic oxygen in the F-region of the atmosphere [2]. These charge transfer collisions result in the production of mainly forward fast scattered neutral oxygen atoms, which will then precipitate further into the atmosphere [3, 4]. The charge transfer cross sections, differential with respect to the product neutral scattering angle, of these collisions provide important information on these precipitations.

Reported in this thesis are the laboratory measurements of absolute integral and differential cross sections (DCS's) for charge transfer of state-selected $O^+(^4S, ^2D, ^2P)$ ions, viz., the ground state $O^+(^4S)$ ions and the undifferentiated metastable state $O^+(^2D, ^2P)$ ions, at energies 0.5, 0.85, 1.5, 2.8, and 5 keV in the laboratory frame with the thermal neutral target gas O_2 over the scattering angular range 0.01^o - 3.50^o. Also reported are the total integral cross sections which were derived for the entire scattering angular range of these same charge transfer reactions. Previously published total charge transfer cross section data for state-selected $O^+(^4S, ^2D, ^2P)$ ions with O_2 are compared with the present derived total integral cross sections.

The method for obtaining an O^+ ground state ion beam from a mixed state beam by employing a filter cell technique will be discussed. The metastable ion DCS measurement is derived directly from a mixed state $O^+(^4S, ^2D, ^2P)$ cross section measurement by appropriately subtracting out the ground state ion contribution to that mixed state

measurement. Due to considerations that will be discussed later, the behavior and magnitudes of the charge transfer DCS's of the two metastable states $O^+(^2D)$ and $O^+(^2P)$ in the keV energy range are believed to be very similar for their reactions with the target gas O_2 and also with the filter gas N_2. If these cross sections are in fact very similar, then it would be very difficult to differentiate between these two low-lying metastable states. In this experiment only two differentiable states were detected in the O^+ mixed state ion beam, which could only be attributable to the ground state $O^+(^4S)$ ions and the undifferentiated metastable state $O^+(^2D, ^2P)$ ions.

2. Experimental Method and Apparatus

A. Charge Transfer Differential Cross Section Formula

The entering ion current (I_0) from a collimated flux (R_0) of monoenergetic ions A^+ into an aperture of area (a) is given by the relationship $I_0 = R_0 a$. The entering ion current then passes through a cell of thickness dx which is filled with a dilute gas of a neutral particle species B. There will be some collisions of the fast projectile ions with the thermal neutral target particles in the cell that will result in a charge transfer process such that:

$$A^+ + B \rightarrow A + B^+. \tag{2–1}$$

The number of gas target centers in this cell of thickness dx is $n(x)adx$, where $n(x)$ is the target gas number density. Then the total charge transfer cross sectional area presented by the target cell gas is $\sigma n(x)adx$, where σ is defined here as the charge transfer cross section. The exiting ion current from the cell of thickness dx then is $R_0(a - \sigma n(x)adx)$. The equation for the entering current minus the exiting current is then given by,

$$I(x) - I(x+dx) = I(x)\sigma(\Omega)n(x)dx. \tag{2-2}$$

Now the term $I(x+dx)$ in Eq. (2-2) can be Taylor series expanded to first order, which will then give the simple differential equation:

$$\frac{dI(x)}{I(x)} = -\sigma(\Omega)n(x)dx. \tag{2-3}$$

Then solving this differential equation for the exiting ion current I(x=L) = I after it traverses a gas cell of length L yields:

$$I = I_o \, e^{-\sigma(\Omega)\int_0^L dx n(x)}. \tag{2-4}$$

We want to solve for $\sigma(\Omega)$ in terms of the incident current I_0 and the scattered product neutral current $N(\Omega)$. Then by substituting in the obvious relationship for I as (I_0 - $N(\Omega)$), i.e., the incident ion current minus the product neutral current into Eq. (2-4) and solving for $\sigma(\Omega)$, one obtains:

$$\sigma(\Omega) = -\frac{1}{\int_0^L dn(x)} \ln\left(1 - \frac{N(\Omega)}{I_o}\right). \tag{2-5}$$

By differentiating Eq.(2-5) with respect to product neutral scattering solid angle Ω, one can get the discrete approximation equation for the charge transfer differential cross section to be:

$$\frac{d\sigma(\Omega)}{d\Omega} = \frac{1}{\int_0^L dn(x)}\left(\frac{1}{I_o - N(\Omega)}\right)\frac{\Delta N(\Omega)}{\Delta\Omega}. \tag{2-6}$$

The length (L) of the target cell (TC) is of the order of 1 mm. The diameter of the entrance aperture to the TC is 20 μm and the exit aperture has a diameter (d) of 200 μm. Therefore the target gas will mostly effuse out the exit aperture, and one would expect a small pressure gradient along the beam axis through the length of the target cell. However, from the consideration that the reduction in $n(x)$ inside the TC is compensated by the increase of $n(x)$ outside of the TC, and from earlier studies in this Lab show, that with a TC ratio of $L/d \approx 5$, then the approximation of $n(x)$ as a constant n as measured by the capacitance diaphragm gauge on the side of the TC is good to within about 1% [5, 6], so that:

$$\int_0^L dx n(x) \approx nL. \tag{2-7}$$

It is further assumed the scattering of the product neutrals to be symmetric about the beam axis in the azimuthal angle ϕ, since the collisional reactants were not polarized. So the angular dependence of the cross section is dependent only on the polar angle θ. Thus Eq (2-6) becomes:

$$\frac{d\sigma(\theta)}{d\Omega} = \frac{1}{nL}\left(\frac{1}{I_o - N(\theta)}\right)\frac{\Delta N(\theta)}{\Delta\Omega}. \tag{2-8}$$

The method in which the differential charge transfer cross section data is acquired and analyzed will be described in detail in the subsequent sections.

B. Basic Overview

A schematic of the apparatus used for measuring the differential and integral charge transfer cross sections is shown in Fig. 2-1. Ions are formed in a medium-pressure arc discharge magnetically confined plasma source. The O^+ ions are formed by introducing O_2 gas in to the source chamber, where a 50 mil tungsten filament is resistively heated and an arc voltage, generally about 60 - 80 V, is applied across the hot filament to the exit aperture plate. Ground state $O^+(^4S)$ ions and the metastable states $O^+(^2D)$ an $O^+(^2P)$ with radiative lifetimes of 3.6 h and 4.57 s respectively [7], are thus formed along with other ion species in the arc plasma by electron impact in the ion source chamber where an external axial magnetic field is applied. The ions effuse out of the ion source chamber exit aperture and then are extracted and focused to be parallel to the z axis by employing an ion optics unit from an electron gun model SW-732Z Southwest Vacuum Devices. The ions are accelerated to the desired keV collision energy by an axial electric field. The resulting ion

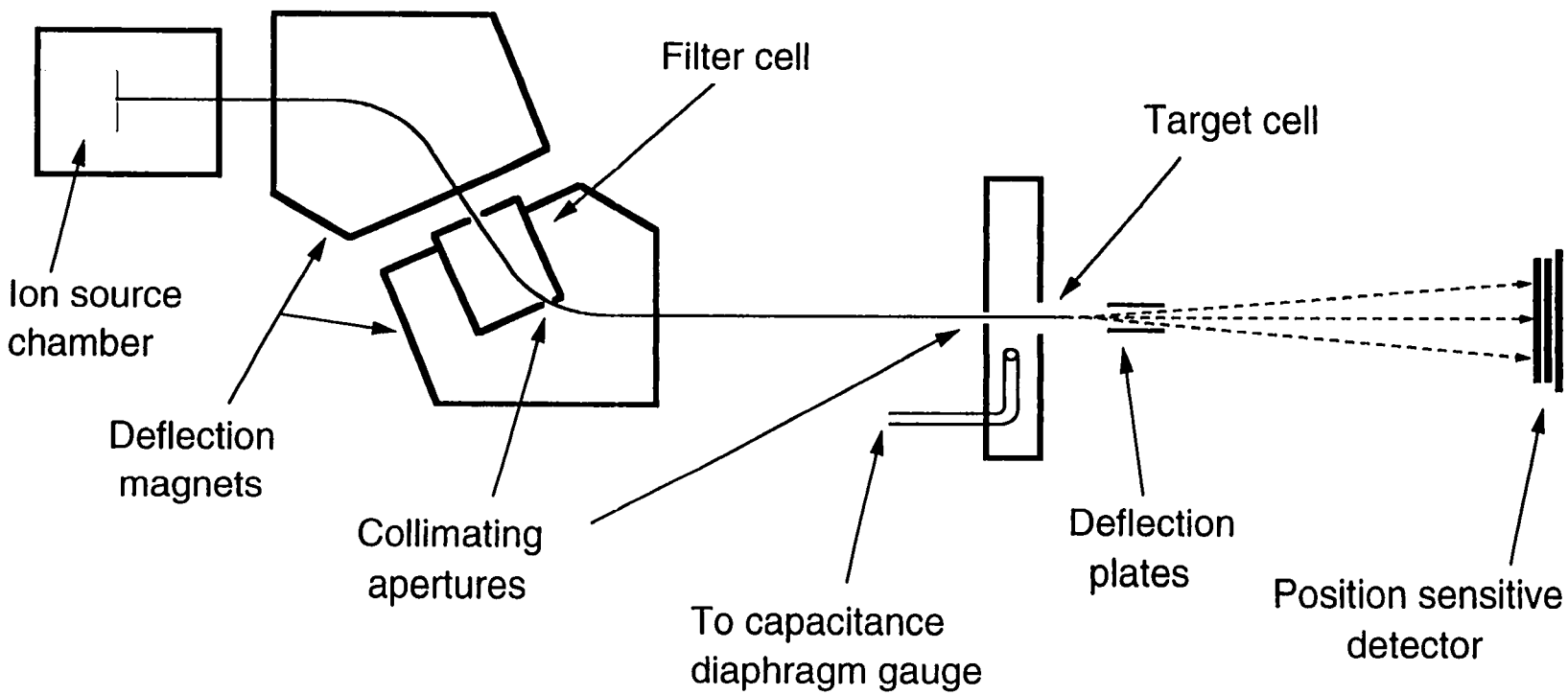

Figure 2-1. Schematic diagram of the apparatus.

beam is found to be monoenergetic with an energy spread of only a couple of eV. The O^+ ions are mass to charge ratio selected by two bending 60^o sector magnets that gives a mass to charge ratio resolution $\Delta m/m \approx 0.01$ [8]. The Filter Cell (FC) is used to electronic state select the $O^+(^4S)$ ions from the $O^+(^4S, ^2D, ^2P)$ mixed state beam. The FC and its technique will be described in detail in a later section. The beam is collimated by directing it through two apertures of 100 μm and 20 μm respectively, with a separation distance of 25 cm, which gives a maximum angular beam divergence of less than 0.016^o.

The ion beam after passing the second collimating aperture enters into the TC and traverses the length of the TC, whose length of about 1 mm is determined by a microscope and micrometer to a precision of 1%. The target cell gas pressure is monitored by a MKS Baratron capacitance diaphragm gauge and it is controlled by a variable leak valve. Thin target conditions, i.e., single collision conditions are obtained in the TC when the decaying exponential in Eq. (2-4) can be accurately approximated to first order as $(1-\sigma nL)$, where the quantity nL is defined as the target thickness (τ). Typical operating O_2 gas pressures in the thin target regime for the TC in this experiment were of the order of about 10 mTorr, which gave a target thickness of about 1 mTorr•cm. The small attenuation of the ion beam by charge transfer in the TC with this target thickness resulted in the production of a forward scattered fast neutral current with a magnitude of about 3.5% of I_o, and consequentially the diminished ion current exiting the TC had a magnitude of about 96.5% of I_o. Outside of the TC in the main chamber, the vacuum pressure is maintained by an oil diffusion pump to be about 3.5×10^{-7} Torr, and the intervening distance between the TC and the PSD is 26.6 cm, then τ for this region is about 1/100 of that found in the TC. It is to be noted that the approximation of the exponential in Eq. (2-4) as $(1-\sigma nL)$ is only accurate to 1.8% for these thin target conditions that resulted in a 3.5% attenuation of I_o. So the direct calculations of the DCS's and integrals in this work were done by using the exact expressions as calculated in Eq. (2-5) and Eq. (2-8)

The ion and scattered neutral currents along with the individual neutrals' impact positions are measured by the PSD, the position sensitive detector, which is located in the main chamber 26.6 cm from the TC. It is assumed the neutral impact position distribution's center of mass is at the scattering angle $\theta = 0$, then the scattering angle θ of a fast neutral product is determined by the simple geometric relationship $\theta = \arctan(r / TC\text{-}PSD)$, where r is the radial distance of the individual neutral's impact position on the PSD as measured from the neutral impact position distribution's center of mass, and TC-PSD is the distance between the TC and the PSD.

The PSD as depicted in Fig. 2-2 consists of two 25 mm diameter active area micro-channel plates with a resistive anode. The micro-channel plates (MCP's) each have over 10^6 15 μm diameter slanted channels covering ~55% of the entire active area of the plates. The channels are slanted by 5 degrees from the normal of the MCP surface. Briefly, a fast particle ion or neutral impacts into one of the channel's wall and causes secondary electrons to be ejected from the wall surface. The PSD is biased by about a couple of thousand volts to produce an electric field, normal to the MCP surface, that will accelerate the secondary electrons towards the resistive anode. The accelerated secondary electrons inside the channel will then collide with the channel wall which will cause additional secondary electrons to be ejected, which in turn will result in more collisions and more additional secondary electrons to be ejected from the channel wall and be accelerated towards the anode. This process is repeated many times inside the channel resulting in a secondary electron cascade traveling towards the anode which gives a gain of more than 1000 electrons for an individual MCP per incident impact event. A total gain of about 10^7 electrons per incident impact event is achieved by stacking the two MCP's as shown in Fig. 2-2. Also there is a voltage on the front of the PSD that is set at -50 V to reject secondary electrons produced from particle impact on the interchannel front surface, this results in some loss of detection efficiency but enhances spatial resolution [9].

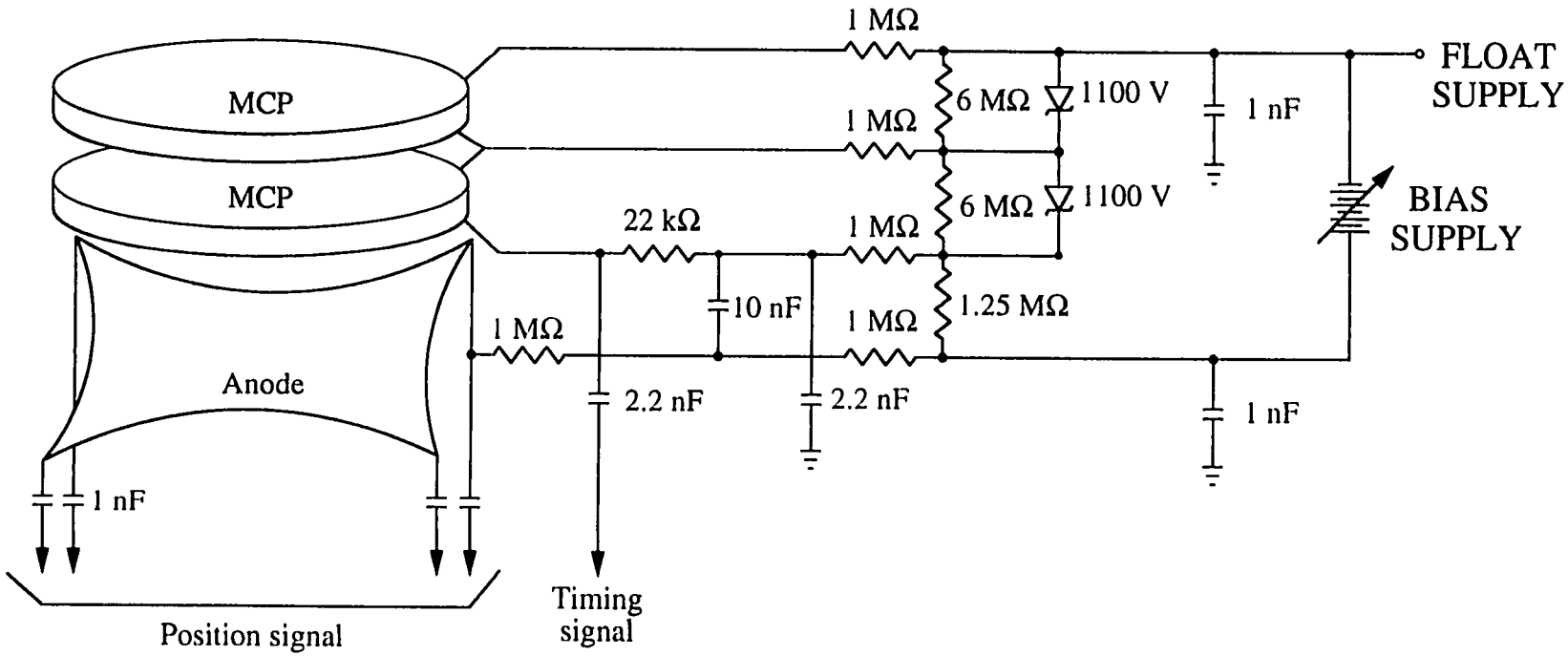

Figure 2-2. Schematic diagram of the PSD and its biasing circuit.

This charge pulse or cloud of about 10^7 electrons is then collected on the resistive anode, and the charge is divided among the electrode contacts on the four corners of the resistive anode in proportion to the proximity of the charge cloud. Thereby, allowing the centroid of this charge cloud to be determined by comparing the sums and ratios of the resulting four corner voltages by the detector and the 2401B Position Analyzer Quantar Technology Imaging Detector electronics unit, which gives a 8-bit X and 8-bit Y digital output of the XY position of the incident impact. This data is then incremented into the appropriate element of a 256 by 256 XY histogram on the Quadra computer in the Lab. This digital data output of the incident impact position gives a linear resolution of 103 μm for the PSD.

The scattered neutrals' incident impact positions on the PSD are detected, and the counts per second are also measured to determine the currents of the scattered neutrals(θ) and the incident ions. As stated earlier the incident ion current density is much larger than the product neutral current density, and it is known that the PSD detection efficiency is dependent on the particle count rate per unit detector area and also on the PSD bias. To make an accurate DCS measurement then the detection efficiencies of these two different current densities need to be the same for a given operating PSD bias. To find the PSD bias where both the ion and neutral fluxes will be detected with the same relative detection efficiency is accomplished by first measuring for each constant particle input flux the count rate of valid impacts detected on the PSD as a function of the PSD bias. The shape of these two curves depends on the settings of the upper- and lower-level discriminators of the PSD electronics and the magnitude of the charge pluses exiting the second MCP. More specifically, a centriod computation will not be made for a charge cloud that impinges on the PSD anode if the sum of the 4 input current pulse-heights are too small or too large as set by the upper- and lower-level discriminators of the PSD electronics to yield an accurate detection of an incident particle's impact position. The resultant curves of the measured

count rate versus PSD bias for the ion flux and for the neutral flux are then normalized by setting the maximum peak of each curve to unity. The point of intersection of the two normalized curves where both have the same relative detection efficiency then determines the operating bias for the PSD at a given ion beam energy.

The detection efficiency of particle also depends on whether the individual particle is an ion or is a neutral. However, keV ions and keV neutral particles are assumed to be detected by the PSD with virtually the same efficiency. Specifically, the detection efficiency depends on the secondary electron ejection coefficient γ^+ for ions and γ^0 for neutrals when the particles hit the channel wall. The difference in the detection efficiencies has been observed previously in this Lab to give an uncertainty in the detection efficiencies of the ions and neutrals at different keV energies to be the same within 3% for 5 keV, 5% for 1.5 keV, and 10% for 0.5 keV [10, 11]. It is to be noted that the currents $\Delta N(\theta)$, I_0, and $N(\theta)$ are not detected absolutely. However, since the currents are in the form of a ratio in the DCS Eq. (2-8), and all other quantities are measured absolutely, then the DCS measurements for this experiment are then measured absolutely.

The measurement of a charge transfer DCS is obtained by measuring the signals of $\Delta N(\theta)$ and I_0 as detected on the PSD. The signal of $\Delta N(\theta)$ is only fraction of I_0, so the measurement of $\Delta N(\theta)$ is somewhat susceptible to the small spurious signals collected on the PSD due to background effects. A background file is then taken first to account for and subtract out any background signals collected on the PSD during a latter scattered signal measurement file. A background file is taken with no gas in the TC for collecting the background signal. The ion beam of about 2 kHz is deflected away from the PSD by applying a transverse electric field between two deflection plates placed after the exit aperture of the TC. And the background signal of about 4 Hz is then measured on the PSD. The background signal consists of two main parts: aperture and residual gas

scattering which together have a count rate of about 2 - 3 Hz; and another 1.8 Hz due to random noise(the dark current).

A charge transfer scattering data file is then taken, where typically a 2 kHz ion beam passes through the neutral target gas in the TC. Thin target conditions are obtained in the TC as described earlier, and again the ions emerging from the TC are deflected away, while the scattered neutral products(θ) are collected on the PSD where their positional data is incremented in the appropriate elements of a 256 by 256 XY array, and their total current is logged. During both these scattering and background files every 20 seconds the primary signal rate is sampled for one second by switching off the deflection plates and measuring both the ions and the background counts for the case of the background file, and measuring the ions and the neutrals + background counts for the case of the scattering file. The incident ion beam width as measured on the PSD is about 200 μm FWHM for this experiment. The positional data for the ions is not necessary for a charge transfer DCS measurement, and in general it is not taken. And further, an energetic 2 kHz point beam can damage the PSD over time. This problem is obviated by rastering the exiting ion beam from the TC with two extra sets of deflection plates into roughly a 5 mm by 5 mm square on the PSD while sampling the primary current.

The scattering file is corrected for the background effects by appropriately subtracting it by the background file. The currents measured from the primary signal and neutral signal must also be corrected for the dead-time generated by the XY positional electronics calculation, which is 10 μs. The true rate (r_t) can obtained from this obvious relationship $r_t = r(1+r_t*\text{dead-time})$, which is derived from a Poisson distribution [12], to give $r_t = r/(1-r*\text{dead-time})$. The ion beam intensity will fluctuate and drift over time, therefore to measure I_0 it must be sample often and quickly. This is done by considering the corrected primary signal current, i.e., the current due to both the undeflected ions plus the scattered neutrals products, to be essentially equivalent to the entering ion beam current

I_0. In the thin target regime the effect of direct scattering is negligible in so much as the probability of the product neutrals having another collision is small, and although a few percent of the ions may be angularly or elastically scattered by collisions with the target gas the majority of these few scattered ions will still be collected on the PSD. As stated earlier, the neutral current is about 3.5% of the primary current. The acceptance angle of the PSD is 3.67^{o} and it captures the majority of the charge transfer scattered neutrals, so for the uncertainty caused by the neutrals scattered off the PSD and therefore not counted is about 3.5% or less for approximating the primary rate as I_0. This small reduction in I_0 can be compensated by estimating the number of neutrals scattered at angles greater than 3.67^{o} and adding their contribution to I_0. The charge transfer cross section is proportional to the number of scattered neutrals to first order in the expansion of the natural logarithm term $-\ln(1-N/I_0)$ in Eq. (2-5), where $N<<I_0$. Thus by estimating the integral charge transfer cross section for the angles larger than 3.67^{o} by extrapolating the DCS curve at the large PSD angles and then integrating this extrapolated curve with respect to the solid angle $2\pi\sin(\theta)d\theta$ from $\theta = 3.67^{o}$ to $\theta = 180^{o}$, one can infer the fraction of scattered neutrals not collected by the PSD to be then essentially equivalent to the ratio of $\sigma(3.67^{o}\text{-}180^{o}) / [\sigma(0^{o}\text{-}3.67^{o}) + \sigma(3.67^{o}\text{-}180^{o})]$. This extrapolation method for obtaining the integral cross sections off the PSD wil be discussed in more detail in section 3.

Along with the primary current being sampled, the pressure of the TC gas is concurrently measured by a MKS Baratron capacitance diaphragm gauge. The Baratron head is maintained at 45^{o} C while the temperature of the TC gas is at room temperature. The gas pressures measured in the TC are in the low mTorr range, i.e., the low transitional flow range for the target gas of question. So the number density is obtained from the ideal gas law adjusted down by about 3% to account for the effect of thermal transpiration.

The data is analyzed by finding the center of mass of the XY array of the scattered neutrals' impact distribution on the PSD, which with the geometry of the apparatus along

with the neutrals' incident impact positions as described earlier gives the scattering angles for the fast product neutrals. Around the located center of mass, concentric rings are constructed from the 256 by 256 data array bins. Each of these rings has a solid angular width $\Delta\Omega(\theta)$, and the number of neutrals collected in that ring width give the product sum $\Delta N(\theta)$. The discrete nature of trying to analyze these square bins by a differential concentric ring analysis is somewhat alleviated by further subdividing each bin so that the overlapping bins on the ring borders have their bin count divided in proportion to the area contained in each of the two rings. The ring widths vary in order to meet the demands of high angular resolution and good counting statistics .

C. State Selective Analysis of the Primary Beam

The method to analyze the two separable electronic states of the O^+ ions, the ground state(^4S) and the undifferentiated long lived metastable state (^2D, ^2P), is based on a simple attenuation method as used by Turner et al. [13]. The mixed state ion beam is passed through a filter cell of gas, where the filter gas is chosen such that there is a large difference between the O^+ ground state and the O^+ metastable state charge transfer cross sections with the gas.

The predominate product channels for the charge transfer reaction O^+ with N_2 are: for the ground state O^+ ions,

$$O^+(^4S) + N_2(X\ ^1\Sigma_g^+, v''=0) \rightarrow O(^3P) + N_2^+(X\ ^2\Sigma_g^+, v'=0),\ \Delta E = 2.0\,eV; \quad (2\text{-}9)$$

for the first metastable state,

$$O^+(^2D) + N_2(X\ ^1\Sigma_g^+, v''=0) \rightarrow O(^3P) + N_2^+(A\ ^2\Pi_u, v'=1),\ \Delta E = 0.0\,eV, \quad (2\text{-}10)$$

$$O^+(^2D) + N_2(X\ ^1\Sigma_g^+, v''=0) \rightarrow O(^1D) + N_2^+(X\ ^2\Sigma_g^+, v'=0),\ \Delta E = 0.6\,eV; \quad (2\text{-}11)$$

and for the second metastable state,

$$O^+(^2P) + N_2(X\ ^1\Sigma_g^+, v''=0) \rightarrow O(^1D) + N_2^+(A\ ^2\Pi_u, v'=0), \quad \Delta E = 0.0\,eV, \quad (2\text{-}12)$$

$$O^+(^2P) + N_2(X\ ^1\Sigma_g^+, v''=0) \rightarrow O(^3P) + N_2^+(B\ ^2\Sigma_u^+, v'=0), \quad \Delta E = 0.1\,eV. \quad (2\text{-}13)$$

Note that the energy defect for the $O^+(^4S)$ reaction is relatively large at 2.0 eV, while for both the metastable states $O^+(^2D)$ and $O^+(^2P)$ the product channels are essentially in energy resonance with the reactant state. So, the likelihood of the charge transfer reaction, i.e., the cross section, is expected to be much greater for the metastable incident ions with their low energy defect than that for the ground state ions with their much larger energy defect. Fig. 2-3 shows the low lying states of O and O^+.

Previous measurements of the total charge transfer cross sections for these reactions do in fact show a large difference between the ground state and the metastable state cross sections [14]. This makes N_2 an ideal candidate for a filter gas, since it will preferentially remove the metastable state ions from a mixed state beam.

The generic formula given for a two state attenuated beam is:

$$\frac{I}{I_0} = fe^{-nl\sigma_1} + (1-f)e^{-nl\sigma_2}, \quad (2\text{-}14)$$

where f is the fraction of ions in state 1. Since the cross section is much larger for the metastable ions in the case of O^+- N_2, then from observing the above two decaying exponential model, the metastable state ions will be attenuated much more rapidly than the ground state ions. Thus, at sufficient filter cell gas pressure, a greater than 99% ground state ion beam can be easily obtained. However, there will be a significant reduction in the overall beam intensity. This problem of low intensity is compounded when operating at the

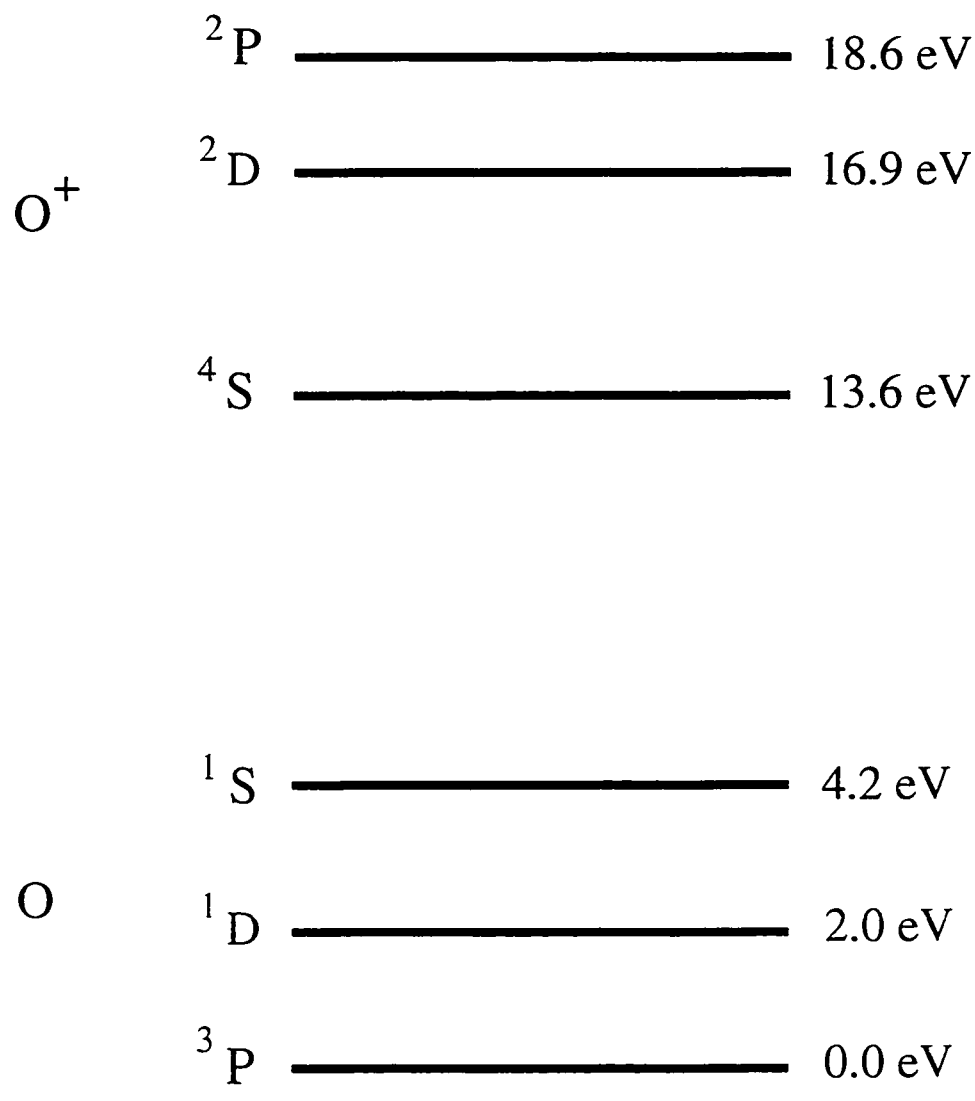

Figure 2-3. Low lying states of O and O^+.

low projectile energy of 500 eV, since the elastic scattering of the ions in the FC becomes now fairly large. Fortunately this is counterbalanced somewhat by the bigger relative difference in the charge transfers cross sections of the two states of the O^+ ions with N_2. Thus a high purity ground state beam was achieved for each ion beam energy examined.

The FC and the first collimating aperture are placed inside the second bending magnet(cf. Fig. 2-1), where the ions necessarily travel in a curved path. Therefore, any product scattered neutrals created in the FC will be removed from the beam, thus insuring that none of the fast O neutrals created in the FC will impact the PSD.

In Fig. 2-4 the effective integral charge transfer cross section of 1500 eV O^+- O_2 in the TC versus the FC N_2 gas pressure is plotted. With no gas in the FC the effective cross section of the mixed state O^+ ions with O_2 was measured at about 11.7 $Å^2$. Then N_2 gas is introduced into the FC and its pressure is increased, which causes the effective integral cross section in the TC to become smaller. This effect is observed because the metastable state ions with their larger cross sections with O_2 are preferentially removed earlier in the FC, since they charge transfer react much more readily than the ground state ions with the attenuating FC N_2 gas to become neutral O atoms in the second bending magnet and thus are removed from the ion beam. As seen in Fig. 2-4 the effective integral cross section in the TC reaches an asymptotic value of about 7.8 $Å^2$ at the FC N_2 gas pressure of about 6 mTorr. This asymptotic value for the cross section is taken to be the value for the ground state cross section. And in this same asymptotic region, the fraction of the ground state O^+ ions in the ion beam exiting the FC is estimated, by a using a two exponential decay model, to be greater than 99%.

After a ground state O^+ beam is achieved by using this filter cell technique, then a differential cross section can be measured as described earlier by taking the scattered signal file and appropriately subtracting it by the background file, and then analyzing the positional data via the previously described differential ring sum method. The metastable

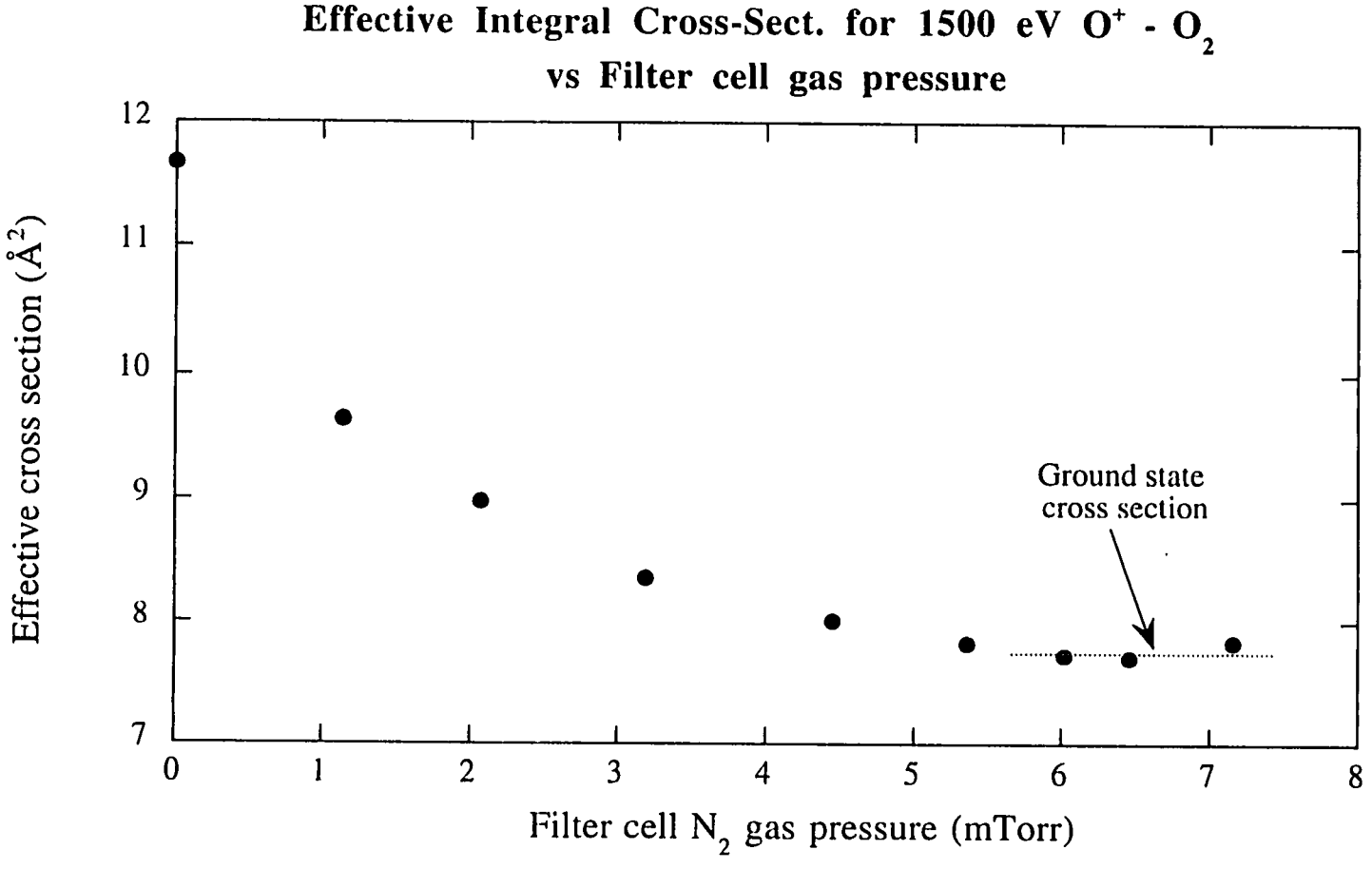

Figure 2-4. Effective integral cross section measurements of 1500 eV O^+- O_2 taken after a mixed state beam passes through the FC at different levels of attenuating N_2 filter gas pressure.

state DCS, then can be gotten by direct subtraction of the ground state DCS contribution from an unfiltered mixed state ion beam DCS measurement by the simple formula:

$$\frac{d\sigma_{ms}}{d\Omega} = \frac{\frac{d\sigma_{tot}}{d\Omega} - f\frac{d\sigma_{gs}}{d\Omega}}{1-f}. \qquad (2\text{-}15)$$

Where f is the fraction of the ground state ions in a mixed state O^+ ion beam and the remaining fraction (1-f) of the mixed state beam is the fraction of the metastable ions. The ground state fraction f in a mixed state beam must then be measured in order to determine the metastable DCS as prescribed by Eq. (2-15).

The procedure for measuring the fractional abundances of the ground state O^+ ions and the metastable O^+ ions in a unfiltered mixed state O^+ beam was refined to be taken as quickly and accurately as possible to reduce the error that is caused by the observed fluctuations in the mixed state O^+ ion beam's composition over a period of time. It was observed on some days the ground state beam fraction in the mixed state beam would relatively change by more than 15% over a period of 1.5 hours. The procedure that was used to make a metastable DCS measurement, was to first take a fraction measurement for 10 min., next make a mixed state DCS total measurement for 30 min., and then take another 10 min. fraction measurement, etc.. The fractions measurements before and after the mixed state DCS measurement were averaged and were normally within 7 percent of each other since the total time to make a single metastable state measurement was less than an hour.

The fraction f was measured by employing the same attenuation method and formula given by Eq. (2-15) as previously described for the production of a pure ground state beam. In this case, the measurement of I/I_0 is measured on the PSD by using the TC as the attenuation cell filled with the attenuating N_2 gas. A semi-log plot of I/I_0 vs. TC gas

pressure was made and the curve was fitted to Eq. (2-14), with the three parameters f, σ_{gs}, and σ_{ms}. Fig. 2-5 is plot of just such a attenuation curve of I/I_0 vs. TC N2 gas pressure for a 1500 eV O^+ mixed state ion beam, which gave the value for the relevant fitting parameter f, the ground state ion fraction, as 0.62. The fraction attenuation curves in general give very reproducible results for the ground state ion fractions with a fitting precision uncertainty for the parameter f of only about 5%. The measurement of I, the ion current after the ion beam passes through the attenuating N_2 gas in the TC, is made by measuring the primary (ions plus neutrals) current on the PSD, while concurrently sampling the neutral count rate by deflecting the ions away from the PSD. Thus the ion current is simply the primary current minus the neutral current. The incident ion current I_0 was approximated to be the primary current as was done for the DCS measurements. So I/I_0 was approximated to be given by the ratio (p-n)/p, i.e., (primary current - neutral current)/(primary current).

One requirement for this approximation to be correct, is that the DCS's for the elastic scattering of both the ions and neutrals off the PSD($\theta > 3.67^o$), need to be the same. Measurements of the elastic scattering of O^+ on N_2 were done to 3.67^o at O^+ energies 0.5 keV and 1.5 keV, and were compared with results done previously in this lab for the elastic scattering DCS's of O on N_2 at 0.5 keV and 1.5 keV [15]. The DCS's of the atomic oxygen neutrals and ions at 1500 eV both coincided with each other as to become virtually indistinguishable well before 3.67^o point marking the outer edge of the current PSD setup, therefore indicating the two DCS's to be the same off the PSD. At the ion energy 500 eV, the same effect is noticed but the overlapping of the two DCS's occurs somewhat closer to the edge of the current PSD edge angle of 3.67^o. For projectile energies greater than 1.5 keV, it was assumed the elastic scattering of neutrals and ions would also be the same for the region off the PSD since the larger kinetic energies of the projectiles would certainly dominate more in the direct scattering processes.

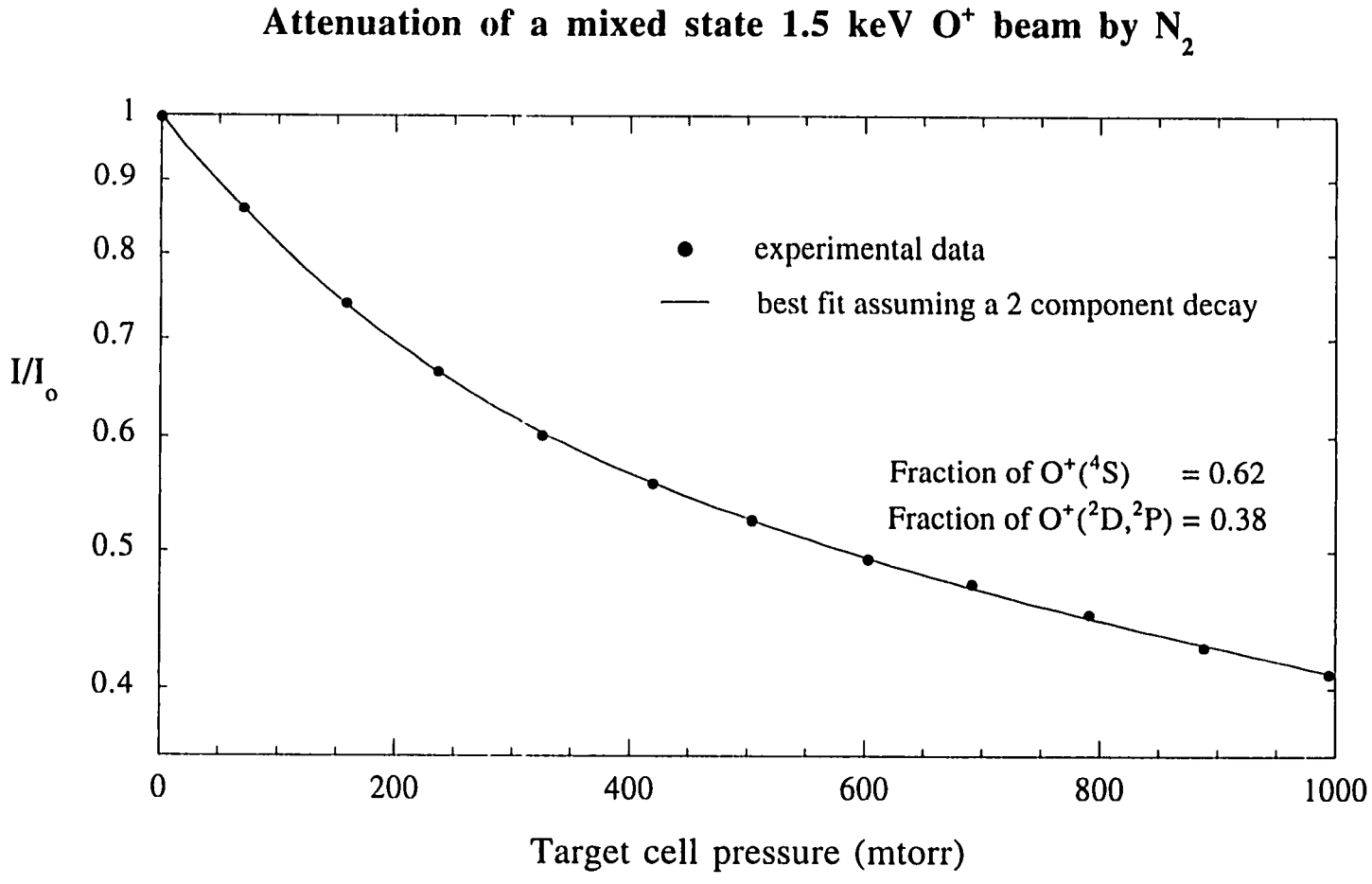

Figure 2-5. An attenuation curve of a mixed state 1500 eV O^+ beam by N_2 gas in the target cell, which from the fitting Eq. gives the incident fractions of the ground state and metastable state ions.

The numerator (p-n) measures the ion current (I) by subtracting the neutrals from the primary count. As mentioned earlier, there is an uncertainty in the relative detection efficiencies being the same for the keV ions and product neutrals, so the error in measuring the current by subtraction can be given by the error equation,

$$\frac{\bar{n}}{(\bar{p}-\bar{n})} \times (\text{detection uncertainty}). \qquad (2\text{-}16)$$

The ratio of the typical mean values, in the above equation, gathered from the attenuation curves multiplied by the detection efficiency uncertainty gives the uncertainties of measuring the ion current on the PSD for the O^+ projectile energies 500 eV, 1.5 keV, and 5 keV as 7%, 6.3%, and 7.5% respectively.

The denominator approximation, $p \approx I_0$, was made as was done previously for the DCS measurement, but, the gas pressures in the TC are no longer held in the thin target regime. The gas pressure in the TC for a fraction measurement is incremented up to that of 1 Torr, while the conditions for a thin target in the TC are of the order of 10 mTorr. This complication indicates, that while the elastic scattering rates off the PSD for the ion and neutrals should cancel and give a good approximation for the ratio, there is no compensating rate loss of ions for the now significant rate of neutrals lost off the PSD due to just the charge transfer scattering processes in the thick target regime. Thus this approximation $p(\text{ion+neutrals}) \approx I_0$ appears to be somewhat flawed. Extensive tests were made to check the self consistency and overall accuracy and precision of this approximated fraction method. Since the metastable DCS measurement is highly dependent on the mixed state beam parameter f, then one self consistency test was to make and compare metastable DCS measurements derived from mixed state beams that had significantly different values for f.

The ground state fraction f is known to be highly dependent on source parameters in this lab. First a metastable DCS measurement was made under normal source conditions where the source chamber was filled O_2 gas at a pressure of 150 mTorr. This produced a mixed state beam with an average value of f=0.63. Then the source parameters were varied by filling the chamber with O_2 gas and N_2 gas at partial pressures of 150 mTorr each. The N_2 gas in the source acted again as a filter gas, thus giving the emergent ion beam a larger ground state fraction. The mixed state beam thus produced was measured to have a significantly higher average value of f=0.80, and again a metastable DCS measurement was taken. The magnitudes of these two metastable DCS measurements were found to be within less than 3% of each other.

A further test was to check the overall consistency of the attenuation fraction method by plotting and fitting the approximated I/I_0 vs. TC gas pressure for a known single state component beam, then on a semi-log plot one would expect to get a straight line. A ground state He^+ ion beam was produced in the source as described previously, but with the arc voltage set to 36 V. Therefore the accelerated thermionic emitted electrons would have energies below 40.5 eV, the energy required to produce the first lowest lying excited state of He^+. The attenuation of the 1500 eV He^+ ion beam with thermal neutral He in the TC, as a function of the He pressure, did indeed produce a straight line as shown in Fig. 2-6, thus demonstrating only a single component beam was observed by this method.

It should be noted here that secondary processes such as stripping, i.e., electron loss of the keV product neutrals is of consideration now, since the gas pressures in the attenuating TC are no longer in the single-collision regime for the fraction attenuation curves. However, the electron loss cross section for the ground state He - He at 1.5 keV is very small at about 0.01 $Å^2$ [16] as compared to the He^+- He charge transfer cross section of about 8 $Å^2$ [17]. A similar semi-log plot of an attenuation curve was made for the single

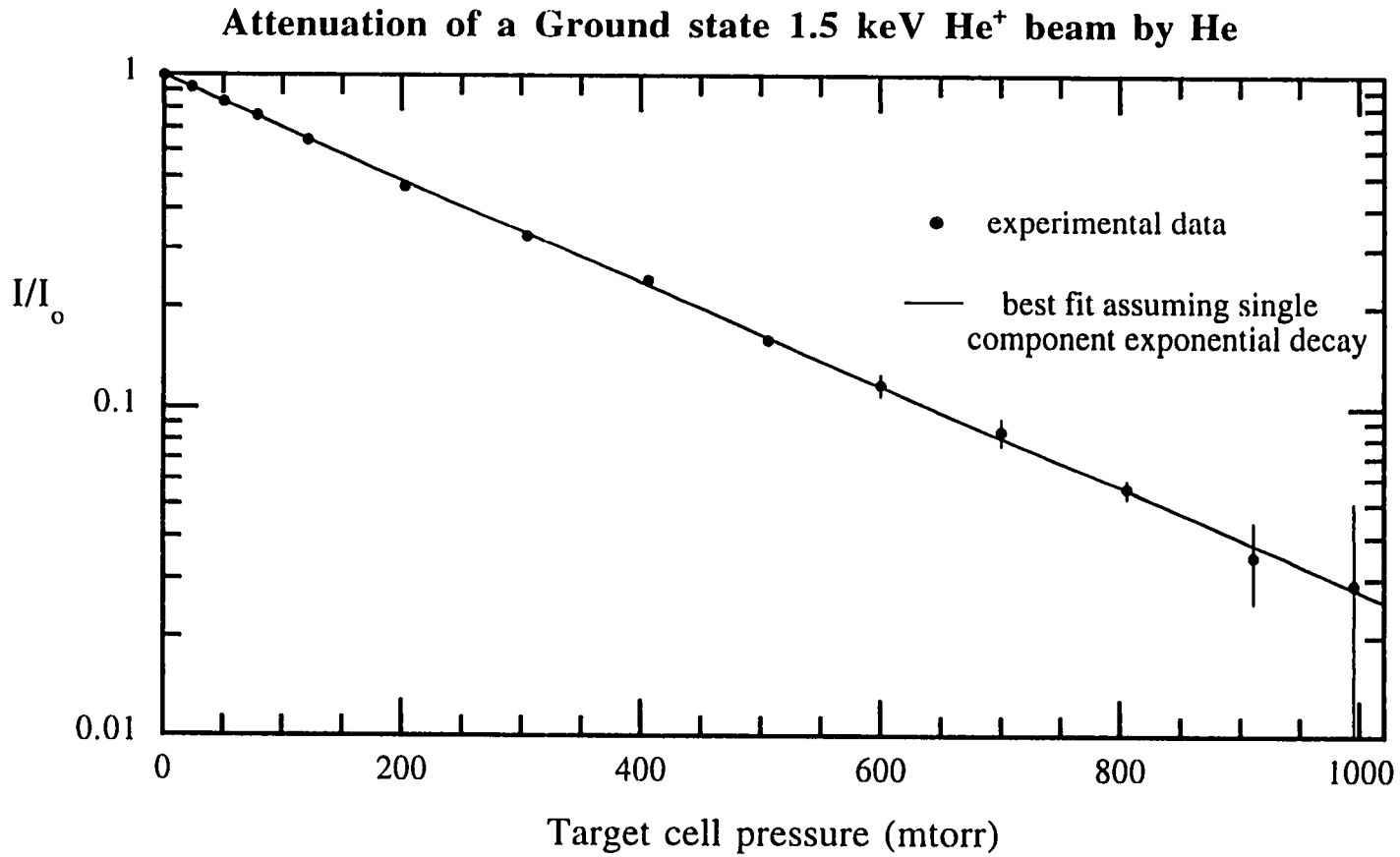

Figure 2-6. Attenuation of a pure ground state 1.5 keV He^+ beam by He gas in the target cell, which is fitted to a single exponential decay equation.

state H^+- H_2 reaction. The plotted curve for H^+- H_2 starts off as a straight line as in the case of He^+- He at the low pressures, but as the pressure increases the line starts to curve up indicating less attenuation of the ion current than predicted by a straight line for a single component attenuation curve. This can be explained by the secondary process of stripping, since the relative difference between the stripping cross section and the charge transfer scattering cross section is much smaller for the case of hydrogen. The H - H_2 stripping cross section is about 0.8 $Å^2$ [18], while the charge transfer cross section is about 5.5 $Å^2$ [17] for keV collisions. So in the high gas pressure region of the curve for hydrogen, then a significant amount of the fast neutrals undergo a stripping collision and become ions again which causes the ion beam to be less attenuated than it would be from the major ion attenuating processes of elastic and charge transfer scattering.

Now for the keV O - O_2 reaction, the stripping cross section appears to be less than 0.1 $Å^2$ [19] and it is assumed that there will also be a similar small stripping cross section for O - N_2. Therefore, considering the magnitudes of the charge transfer cross sections for O^+- O_2 and O^+- N_2 are about 2 orders of magnitude greater than the corresponding stripping cross sections for the neutral projectiles, then the secondary process of stripping should be of negligible effect in the case of the O^+- N_2 attenuation curve method for determining the O^+ ground state ion fraction.

A last test was done by actually measuring I_0 by evacuating the gas from the TC and measuring the unfiltered current on the PSD. This a more difficult and time consuming experiment. Since there are beam fluctuations and drifts in the ionic current, then for the I_0 measurement to be accurate it needs to be taken simultaneously as possible. But now there is a time lag due to the time it takes to effectively evacuate the gas from the TC, which will increase somewhat the uncertainty of this measurement. The oxygen in the ion source consumes the heated tungsten filament fairly rapidly, so the replacement of the existing 750 W 50 A filament power supply to a 1000 W 100 A power supply allowed for a thicker

filament to be used. The filament diameter size was changed for 30 mil to 50 mil, and thus the experiment could be conducted under optimal beam stability conditions for much longer times.

So, the procedure was to run the TC attenuation fraction method as discussed previously, but this time I_o was to be concurrently sampled by evacuating the TC gas at each given gas pressure data point. Hence, one could directly compare both methods. The results of this comparison showed the fraction value given by the (p-n)/p approximation fitting method was found to differ from the fraction value given by the $(p-n)/I_o$ fitting method at three test ion beam energies of 500 eV, 1.5 keV, and 5 keV, by 10%, 4%, and 4% respectively.

These three tests of the approximated fraction method, e.g., the high reproducibility of the integral value σ_{ms} when varying the ground state beam fraction, the single only decay component curve observe when attenuating a pure ground state He^+ ion beam, and the favorable comparison of the ratio (p-n)/p with $(p-n)/I_o$, shows that while the approximated fraction method is somewhat theoretically flawed, it does make reproducible and fairly accurate measurements of f the ground state ion beam fraction.

The measured DCS's of O^+ on the target gas O_2 are reported in this thesis in the next section. The predominate product channels for the charge transfer reaction O^+ with O_2 for the ground state ions are:

$$O^+(^4S) + O_2(X\ ^3\Sigma_g^-, v''=0) \rightarrow O(^1D) + O_2^+(X\ ^2\Pi_g, v'=1),\ \Delta E = +0.9, \qquad (2\text{-}17)$$

$$O^+(^4S) + O_2(X\ ^3\Sigma_g^-, v''=0) \rightarrow O(^3P) + O_2^+(X\ ^2\Pi_g, v'=1),\ \Delta E = -1.1. \qquad (2\text{-}18)$$

The product channels for the first metastable state are:

$$O^+(^2D) + O_2(X\ ^3\Sigma_g^-, v''=0) \rightarrow O(^3P) + O_2^+(a\ ^4\Pi_g, v'). \qquad (2\text{-}19)$$

$$O^+(^2D) + O_2(X\ ^3\Sigma_g^-, v''=0) \rightarrow O(^3P) + O_2^+(A\ ^2\Pi_g, v'), \qquad (2\text{-}20)$$

$$O^+(^2D) + O_2(X\ ^3\Sigma_g^-, v''=0) \rightarrow O(^1S) + O_2^+(X\ ^2\Pi_g, v'=1), \quad \Delta E = -0.2. \qquad (2\text{-}21)$$

There are several vibrational overlaps for the product channels in Eqs. (2-19) and (2-20) at near energy resonance with the reactants. The product channels for the second metastable state are:

$$O^+(^2P) + O_2(X\ ^3\Sigma_g^-, v''=0) \rightarrow O(^3P) + O_2^+(b\ ^4\Sigma_g^-, v'), \qquad (2\text{-}22)$$

$$O^+(^2P) + O_2(X\ ^3\Sigma_g^-, v''=0) \rightarrow O(^1D) + O_2^+(A\ ^2\Pi_g, v'), \qquad (2\text{-}23)$$

$$O^+(^2P) + O_2(X\ ^3\Sigma_g^-, v''=0) \rightarrow O(^1D) + O_2^+(a\ ^4\Pi_g, v'). \qquad (2\text{-}24)$$

There are three fairly large vibration overlaps for channel given by Eq. (2-22), which have energy defects of about -0.2, -0.4, and -0.6 each. For the other two channels in Eqs. (2-23) and (2-24) there are many small vibrational overlaps with energy defects ranging from about -0.4 eV through 1.4 eV.

Inspection of the magnitude of the vibrational overlaps, i.e., the Frank-Condon coefficients, and the energy defects of these product channels, shows that the metastable incident ions have many near energy resonant processes for the charge transfer reaction to take place [14]. The ground state incident ions have less channels with larger energy defects. So from these considerations, it is expected that the metastable ion cross sections to be significantly larger than the corresponding cross sections for the ground state ions, particularly at the lower projectile energies.

The charge transfer product channels of both O_2 and N_2 suggests that the metastable state $O^+(^2D)$ and metastable state $O^+(^2P)$ cross sections to be very similar in each case especially when considering cross sections in the keV energy range. This similarity in the cross sections makes the differentiation of the two metastable states impossible by the attenuation method described earlier. Thus, the beam analysis is limited to a two component O^+ beam consisting of the ground state $O^+(^4S)$ ions and the undifferentiated metastable state $O^+(^2D, ^2P)$ ions.

D. Experimental Uncertainties

Table 2-1 list the factors that contribute to the experimental uncertainties of the charge transfer DCS measurements of the ground state and the mixed state keV O^+- O_2 charge transfer reactions. Table 2-2 lists the factors that contribute to the experimental uncertainties of the derived DCS measurement of the metastable state keV O^+- O_2 charge transfer reactions. The angular uncertainty for the ground state, mixed state, and metastable state reactions all result principally from the primary beam size and the discrete ring width analysis. The uncertainties for the ground state and mixed state DCS's arise primarily from the counting statistics and the difference in the detection efficiency of the scattered neutral products to that of the primary ions. And also for the low projectile energy ground state DCS's, where there is a significant difference in the differential cross section magnitudes for the ground state and metastable state, then these DCS's magnitudes at the small angles will have a slight systematic uncertainty due to a possible small contamination of the order of 1% of metastable ions in the filtered ground state beam. This effect would increase these magnitudes at the small angles by a only a few percent .

The metastable DCS's are derived from a mixed state beam measurement as shown in Eq. (2-15). From examining the weighted error equation along with the magnitudes and uncertainties of the experimental quantities and measurements, then for the metastable DCS's, the primary contributors to the overall uncertainty are found to come from the counting statistics and the difference in the detection efficiency of the scattered products to that of the primary ions in the mixed state DCS measurement, and the magnitude of f which will determine the weight constants in the metastable DCS error equation.

It is to be noted that the error in the counting statistics becomes large in the DCS measurements only for the outer differential rings and thus for the final integral values this statistical contribution to the overall uncertainty will be small. Beside this difference in the statistical counting of the individual differential rings to the now summed value of the

scattered products, all other experimental DCS magnitude uncertainties listed in the tables 2-1 and 2-2 will contribute in a similar fashion to the ground state and metastable state integral values given in the next section.

Table 2-1. Experimental uncertainties for $O^+(^4S) - O_2$ and $O^+(^4S, ^2D, ^2P) - O_2$ DCS's.

Experimental quantity	uncertainty contributing to $d\sigma/d\Omega$
	Magnitude
Scattered products, $\Delta N(\Omega)$	
counting statistics & beam fluctuation	± 3 - 28%
relative detection efficiency	± 3-10%
Primary Ion flux, I_O	
beam fluctuation	± 3%
product loss off PSD	± 0.4 - 3.5%
TC length, L	± 1%
Target gas density, n	
measurement drift	± 2%
thermal transpiration	± 2%
approximate n as constant	± 1%
	Angle
Solid angle, $\Delta\Omega$	
PSD calibration	± 4%
TC - PSD distance	± 1%
Analysis ring width	
varying ring width	$\pm 0.022^o$ - 0.167^o
Beam size	$\pm 0.022^o$

Table 2-2. Experimental uncertainties for $O^+(^2D, ^2P) - O_2$ DCS's.

Experimental measurement or quantity	uncertainty contributing to $d\sigma/d\Omega$
	Magnitude
Differential cross section, DCS	
DCS ground state	± 6 - 29%
DCS mixed state	± 6 - 27%
Fraction of ground state ions, f	
method approximation	± 9 - 14%
parameter fit	± 2 - 16%
	Angle
Solid angle, $\Delta\Omega$	
PSD calibration	± 4%
TC - PSD distance	± 1%
Analysis ring width	
varying ring width	$\pm 0.022^o$ - 0.167^o
Beam size	$\pm 0.022^o$

3. Results and Discussion

A. Differential Cross Sections

Absolute differential cross sections have been measured for state-selected 0.5, 0.85, 1.5, 2.8, and 5.0 keV O^+ ions with the target gas O_2 at the laboratory scattering angles of 0.01^o - 3.50^o. Table 3-1 shows the specific reactions that have been measured.

Table 3-1. The specific charge transfer reactions for the DCS's which were measured.

charge transfer scattering	projectile energy(keV)
$O^+(^4S) + O_2 \rightarrow O + O_2^+$	0.5, 0.85, 1.5, 2.8, 5.0
$O^+(^2D, ^2P) + O_2 \rightarrow O + O_2^+$	0.5, 0.85, 1.5, 2.8, 5.0

The measured O^+- O_2 charge transfer absolute DCS's for both the ground state and metastable state ions at the energies of 0.5, 0.85, 1.5, 2.8, and 5.0 keV are presented in the following figures of Fig. 3-1 through Fig. 3-5.

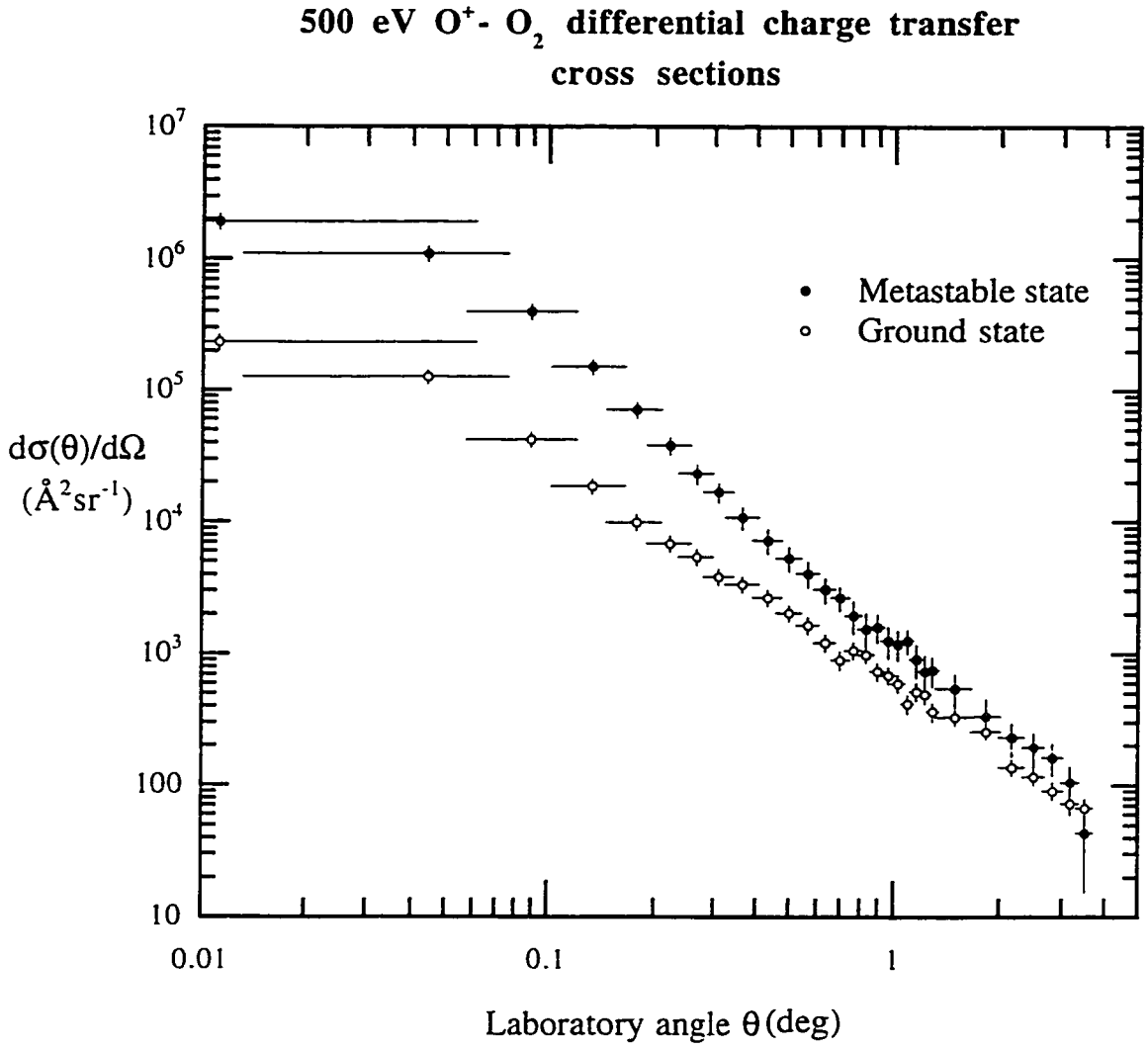

Figure 3-1. Charge transfer differential cross sections versus the polar scattering angle θ for 500 eV $O^+(^4S)$ - O_2 and 500 eV $O^+(^2D, ^2P)$ - O_2.

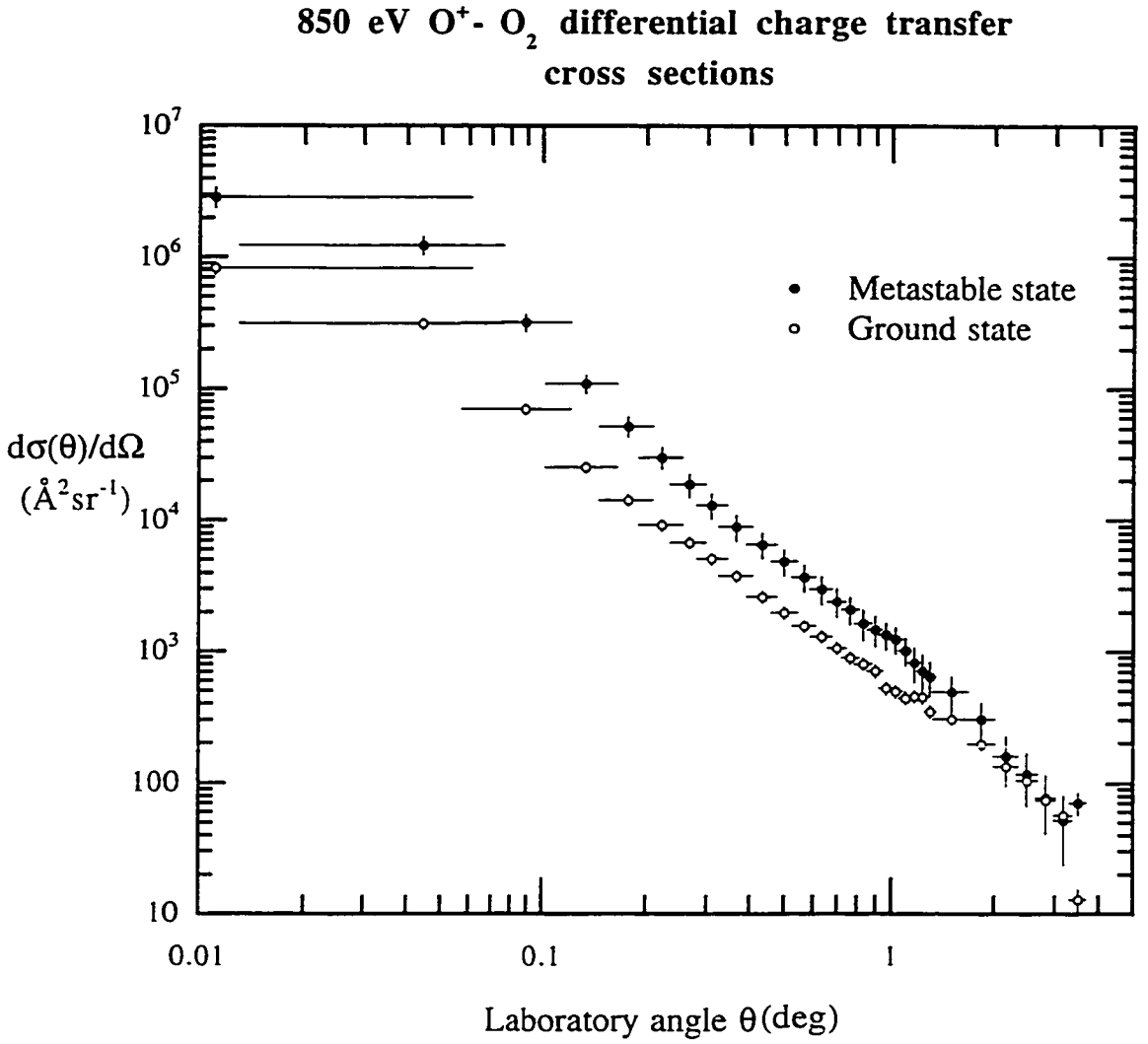

Figure 3-2. Charge transfer differential cross sections versus the polar scattering angle θ for 850 eV $O^+(^4S)$ - O_2 and 850 eV $O^+(^2D, ^2P)$ - O_2.

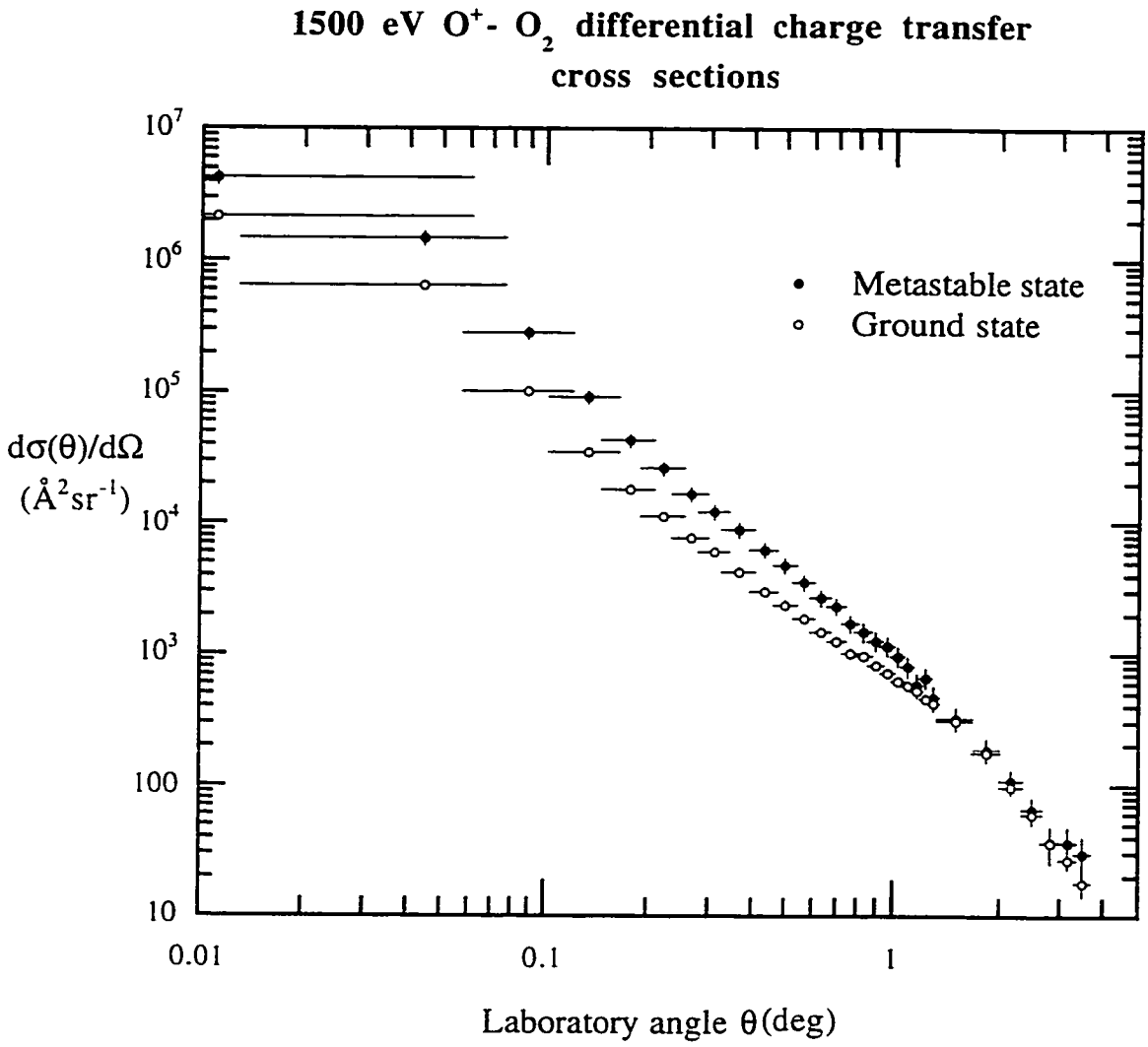

Figure 3-3. Charge transfer differential cross sections versus the polar scattering angle θ for 1500 eV $O^+(^4S)$ - O_2 and 1500 eV $O^+(^2D, ^2P)$ - O_2.

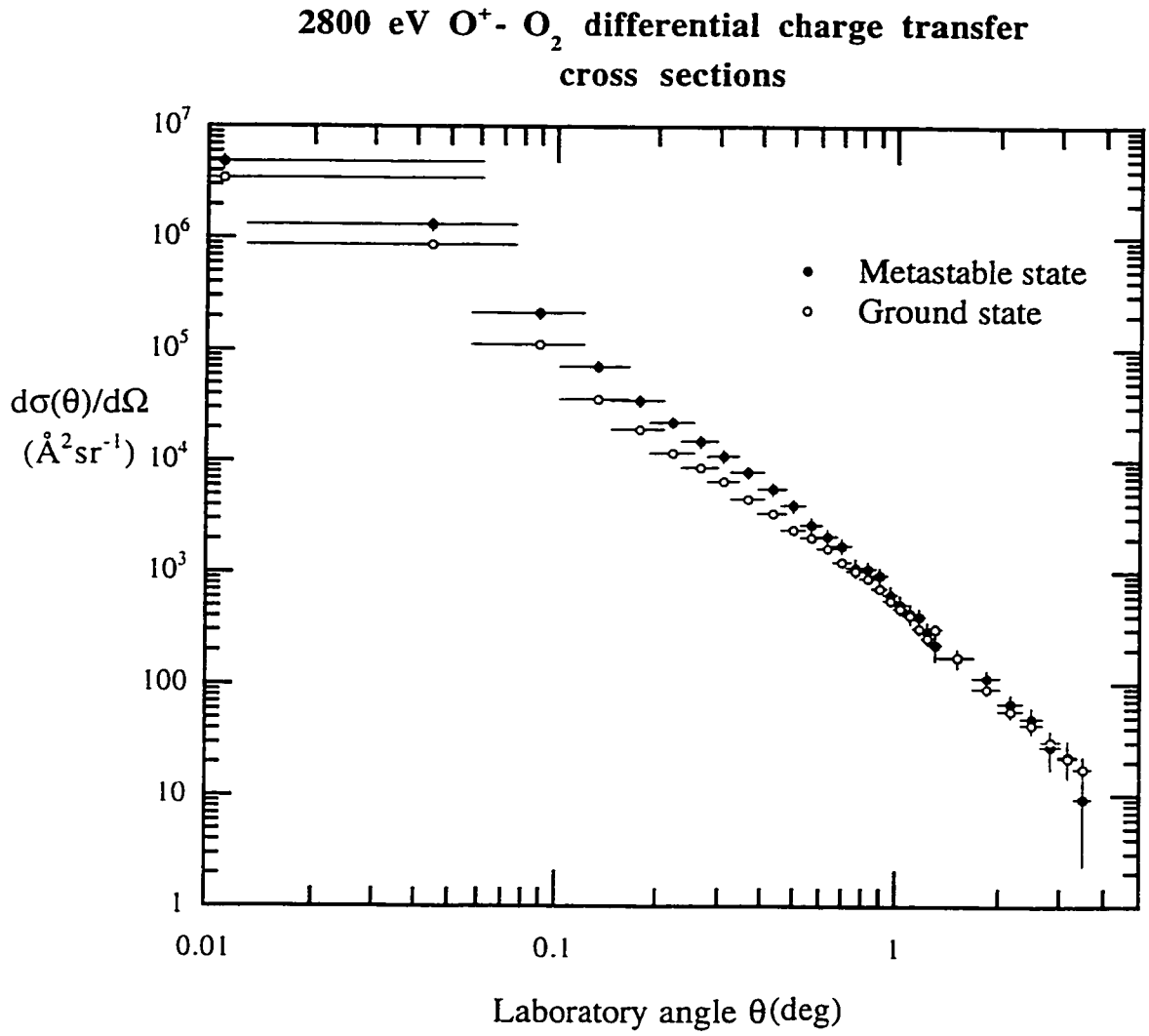

Figure 3-4. Charge transfer differential cross sections versus the polar scattering angle θ for 2800 eV $O^+(^4S)$ - O_2 and 2800 eV $O^+(^2D, ^2P)$ - O_2.

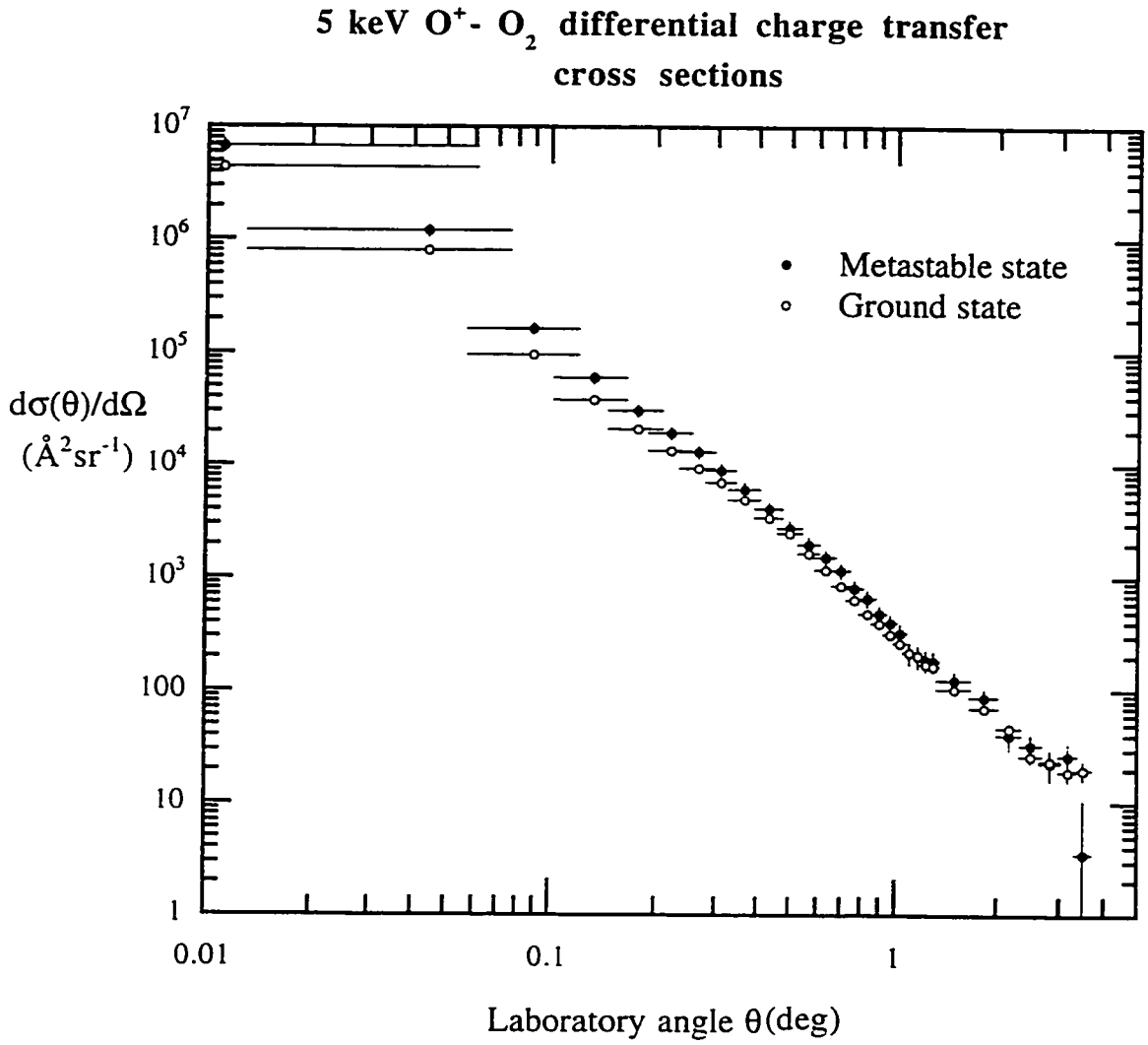

Figure 3-5. Charge transfer differential cross sections versus the polar scattering angle θ for 5.0 keV $O^+(^4S)$ - O_2 and 5.0 keV $O^+(^2D, ^2P)$ - O_2.

The structure of the ground state DCS's are significantly different from that of the metastable state DCS's particularly at the lower projectile energy. The smaller forward shape of the ground state DCS's at the small scattering angles was anticipated from the earlier examination of the relatively large energy defect of about 1 eV as seen in Eqs. (2-17) and (2-18). This energy defect indicated there would have to be harder collisions for charge transfer to occur, which would result in larger scattering angles for the fast product neutrals. The shape for the metastable state DCS's are larger in magnitude and they are more forward peaked than the ground state DCS's at the smaller angles, which can be explained by there being many near resonant channels given by Eqs.(2-19) - (2-24) for the charge transfer reaction to occur. Thus, charge transfer can then occur more readily at the larger impact parameters resulting in smaller scattering angles for the fast product neutrals. Also, as the kinetic energy of the projectile increases to 5 keV the shape and magnitude for the ground state and metastable state DCS's became more similar as expected.

B. Integrals and Total Cross Sections

The absolute integral charge transfer cross sections were obtained from the integral cross section formula as given by Eq. 2-5 for the state-selected 0.5, 0.85, 1.5, 2.8, and 5.0 keV O^+ ions with the target gas O_2 over the extended angular range $\theta = 0^o$ to $\theta = 3.67^o$. The cross sections at $\theta = 0^o$ were tacitly assumed to be zero. This assumption is based on the classical scattering model and was made since the finite width of the primary ion beam and the limited resolution of the PSD prohibited the possibility of making an accurate measurement of the scattering signal at the zero angle point. So the integral cross sections reported here are just due to the ratio of the sum of the scattered neutral signal for the entire active surface of the PSD to the primary ion signal, where the present maximum collection angle of the PSD is $\theta = 3.67^o \pm 0.16^o$. It is instructive to note that these integral cross section values obtained from the exact analytical expression given by Eq. 2-5 are

equivalent to the appropriate Riemann sums of the DCS(θ_i's) values given by the discrete approximation formula Eq. 2-8 with respect to $\Delta\Omega_i$, i.e., $2\pi\sin(\theta_i)\Delta\theta_i$, where the θ_i's for the DCS(θ_i's) values reported are to be considered at the corresponding midpoint of their respective $\Delta\theta_i$ intervals. Then is to be understood that the angular range of 0.01^o - 3.50^o reported for the DCS's correspond to the midpoint values of θ in the discrete concentric solid angle intervals of $2\pi\sin(\theta_i)\Delta\theta_i$ for the total angular range of 0^o - 3.67^o. The Riemann sum would appear as:

$$2\pi\sum_i \frac{d\sigma(\theta_i)}{d\Omega}\sin(\theta_i)\Delta\theta_i \qquad \text{Eq. (3-1)}$$

The cross sectional areas at angles greater than 3.67^o were acquired by fitting the large angle DCS's curve regions to a power law as suggested by their linear log-log form, and then integrating the extrapolated fits over the missing angular range of 3.67^o - 180^o. These extrapolated cross section areas were added to the integral cross sections (0^o - 3.67^o) to give the total integral cross sections. Reported in Table 3-2 are the present keV O^+- O_2 absolute integral cross section values for the angular range 0^o - 3.67^o and 0^o - 180^o, and also listed are the total cross sections from prior literature.

The total integral cross sections for $O^+(^4S)$ and $O^+(^2D, ^2P)$ at 0.5, 0.85, 1.5, 2.8, and 5.0 keV with the target gas O_2 are presented in Fig. 3-6 along with previously published results, with the exception of the present 500 eV ground state total integral cross sections which could not be derived by the extrapolation method due to the poor counting statistics in the outermost rings.

The data for the ground state O^+ total cross sections from Moran and Wilcox [14] was obtain by using a controlled electron impact source. So their ground state cross sections should be fairly accurate and they do agree well with the present data presented.

Table 3-2. O^+- O_2 integral charge transfer cross sections and total cross sections from previous literature.

O^+ state and energy		present $\sigma(0^o\text{-}3.67^o)$	present $\sigma(0^o\text{-}180^o)$	Moran & Wilcox σ(total)
^4S	500 eV	4.5 ± 0.6		
^4S	850 eV	5.6 ± 0.5	6.7 ± 1.3	8.
^4S	1500 eV	7.9 ± 0.6	8.2 ± 0.6	8.
^4S	2800 eV	9.1 ± 0.6	9.6 ± 0.7	8.3
^4S	5000 eV	8.9 ± 0.6	9.8 ± 0.7	
$^2D,^2P$	500 eV	18.0 ± 3.0	19.3 ± 3.3	
$^2D,^2P$	850 eV	16.9 ± 3.1	18.2 ± 3.4	32.
$^2D,^2P$	1500 eV	16.2 ± 2.0	16.9 ± 2.1	29.
$^2D,^2P$	2800 eV	14.1 ± 1.8	14.3 ± 1.9	26.4
$^2D,^2P$	5000 eV	12.3 ± 1.6	12.5 ± 1.6	

All cross sections are in $Å^2$.

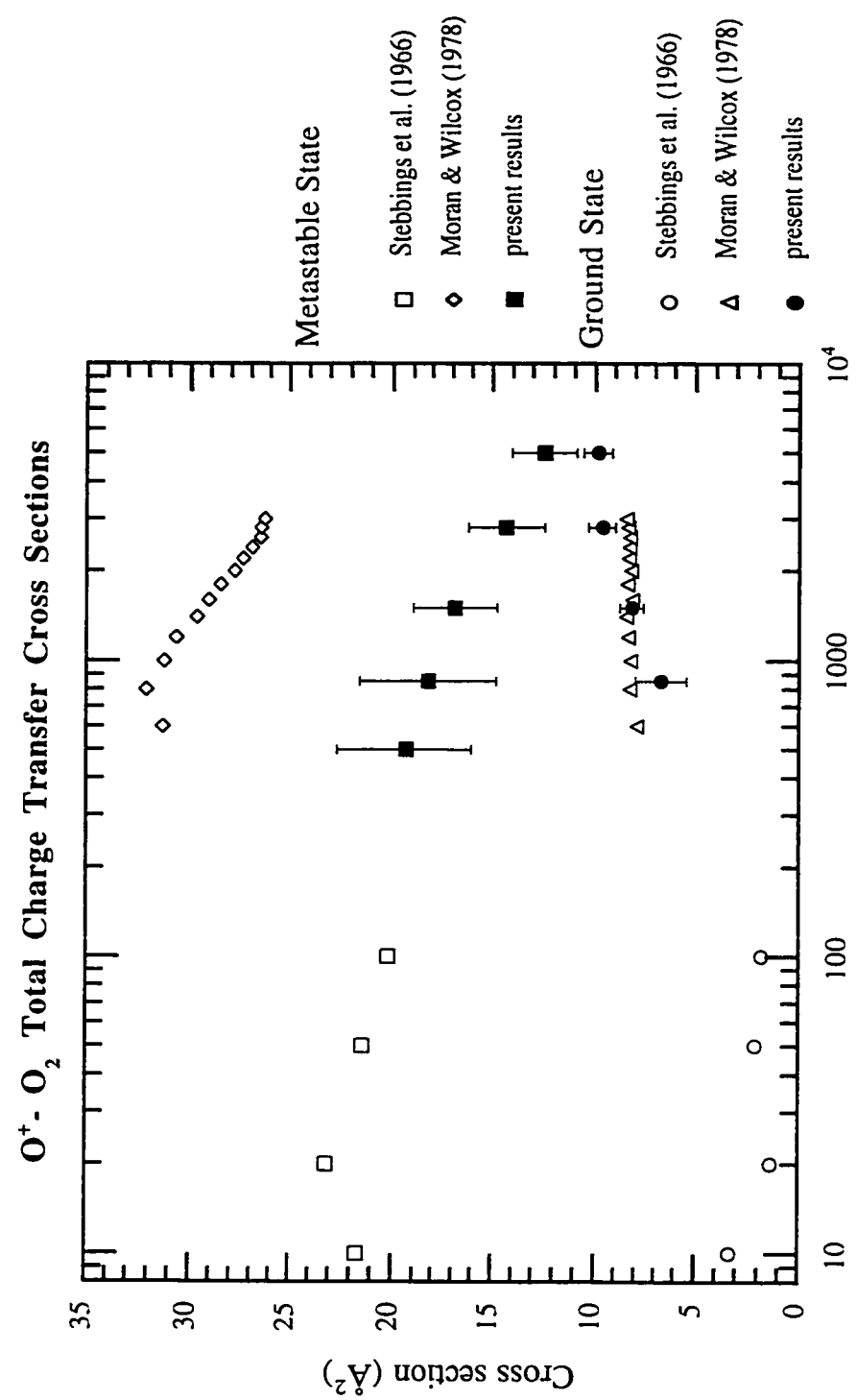

Figure 3-6. Total charge transfer cross sections of O^+- O_2 from present results and prior literature.

However, Moran and Wilcox did not directly measured the beam state fractions but assumed a 70% ground state fraction for all O^+ ion projectile energies based on a previous measurement made in a different lab by Turner et al.[13]. It is to be noted that in this paper by Turner et al. there is no mention of the constancy of the fractions they obtained. So the wisdom of Moran and Wilcox to operate under this assumption seems highly questionable, especially since the experiments in this lab have shown the ground state fraction to be dependent not only on the energy of the ionizing electrons in the source, but also on the source gas pressure, ion extraction and accelerating voltages, and the condition of the heated tungsten filament. Not to mention significant fluctuations in the mixed state beam fractions were sometimes observed over the time period of a few hours or less. This assumed 70% ground state fraction was used by Moran and Wilcox to infer their metastable cross section from a mixed state measurement by subtracting out the ground state contribution. The average ground state fractions measured in this lab during the mixed state cross section measurements of O^+- O_2 at 0.5, 0.85, 1.5, 2.8, and 5.0 keV were 51%, 58%, 45%, 41%, and 31% respectively, which were clearly different from each other and were not at some constant value.

The effect of assuming a constant 70% ground state fraction would increase the metastable state total of the present data, but still the present metastable data would be significantly lower than the data reported by Moran and Wilcox. Since Moran and Wilcox assumed a constant 70% fraction, they could not possibly avoid potential random error introduced by possible significant beam fraction fluctuation caused by random fluctuation or by changing the source parameters in the mixed state cross section measurement. So their assumption of a constant fraction not only introduces a probable systematic error but also has the potential for rampant random error. And this random error could irretrievably distort the final determinations of the metastable state cross sections reported by Moran and Wilcox.

The data from Stebbings et al. [20] is at a lower energy O^+ ion range of 10 - 100 eV. The lower energy metastable cross section data shows a nice continuity in magnitude as a function of projectile energy with the present data at the higher keV energy range. And the present ground state cross sections decrease as the kinetic energy of the projectile, which is supported by Stebbings et al. ground state cross section data at the lower energies.

4. Conclusions and Recommendations

Measurements of the state-selected charge transfer absolute DCS's for 0.5, 0.85, 1.5, 2.8, and 5.0 keV $O^+(^4S)$ and $O^+(^2D, ^2P)$ ions with the target gas O_2 have been presented for the laboratory angular range of 0.01^o - 3.50^o. A high purity ground state O^+ beam was obtained by allowing the mass to charge ratio selected $O^+(^4S, ^2D, ^2P)$ beam to pass through the FC which was filled with N_2 gas. N_2 was chosen as the filter cell gas since it has a much larger charge transfer cross section with the $O^+(^2D, ^2P)$ ions than with the $O^+(^4S)$ ions, and thus it will preferentially remove the metastable state ions from the mixed state beam. The metastable cross sections were derived from a mixed beam state analysis, which entailed the measurement of the fraction of the ions in a mixed state beam that were in the ground state. Then the metastable state cross section could be directly inferred by subtracting out the ground state ions contribution to the mixed state cross section measurement. These differential cross sections, as a function of the fast product scattering angle, are examined for the first time for the different electronic states of the O^+ ions. The magnitudes of the cross sections depended significantly on the electronic state of the O^+ ion, particularly at the low collision energies.

Absolute integral charge transfer cross sections for the laboratory angular range of 0^o - 3.67^o and 0^o - 180^o were reported for 0.5, 0.85, 1.5, 2.8, and 5.0 keV $O^+(^4S)$ and $O^+(^2D, ^2P)$ with O_2, with the exception of the 500 eV ground state total integral cross section. Previously published total cross section measurements were compared to the present results for the total integral charge transfer cross sections of state-selected keV O^+ with O_2. Both previously published measurements of the $O^+(^4S)$ - O_2 total cross sections show good agreement with the present results, where one of the prior measurements is in the comparable keV energy range, and the other data set is in the low 10 - 100 eV projectile energy range.

The $O^+(^2D, ^2P)$ totals for the lower energy data set showed excellent continuity with the present results, while the prior comparable keV data set had significantly higher magnitudes for the metastable total cross sections than the present results. This prior keV data is believed to be suspect. They employed a method similar to the one used here to obtain a metastable state cross section by subtracting out the ground state ions' contribution to a mixed state measurement. However, instead of directly measuring the ground state ion fraction they assumed a constant 70% ground state ion fraction value, which was found in this lab to be highly dependent on source parameters.

The ionic beam composition analysis performed in these experiment to measure the fractions of the ground state and metastable state ions was done by measuring the currents with the PSD, the position sensitive detector. But, this measurement with the beam axis essentially centered on the PSD can only be an approximation of the ratio I/I_o due to the problems caused by the product neutrals in the thick target regime as previously discussed. Of course this problem could be easily remedied by just measuring the currents directly with some type of electrode or faraday cup inside a gas attenuation cell. It is preferable to place the gas attenuation cell after the second magnet to ensure that there will be no contamination from other ion species, and since this cell would be specifically designed for this task, it would have no exposed insulators which could collect charge and thus alter the ion beam.

In order to measure appreciable currents greater than a pA, then this measurement must take place before the beam enters the TC. The ion beam could be deflected from the front of the TC to an attenuation cell place to the side in the main chamber specifically designed to measure the desired current ratio. A 5 cm attenuation cell length would require 50 times less than the highest gas pressure that was used to make an attenuation curve in the TC with its length of ~1 mm. With this type of attenuation gas cell, then the gas pressure times the length, i.e., the thickness of the cell could be made greater while

maintaining a smaller gas throughput to the main chamber than that which was used in the TC.

This increase in the gas cell's thickness would extend the range of the attenuation curve, which would give a more accurate fit for the ground state ion fraction (f), when measuring I_0 directly. And the entrance aperture also could be made relatively large to help collect a steady large current on the electrode situated on the completely closed off backside of the fraction attenuation cell. The electrode in the back of the cell could be floated up to some small positive bias to prevent the escape of secondary electrons emitted from neutral impacts, and thus insure the correct collection of the ion current. One possible way to measure I_0 is to have a second moveable electrode placed just after the entrance aperture of the cell. Therefore, the beam would be essentially unattenuated and an accurate and simultaneous measurement of I_0 could be made by moving the second electrode into the entering beam path.

Other similar experiments measuring the charge transfer cross sections of state selected keV O^+ with thermal neutral molecular gas targets in this lab are planned or have been completed or they are currently in progress for the gas targets H_2, CO_2, and H_20. The experiment planned after these molecular targets is to measure the charge transfer cross sections of keV O^+- O, where O atoms as previously mentioned are the most abundant neutral particles in the regions of the ionosphere where the O^+ precipitating fluxes have been observed.

References

[1] R. G. Johnson, R. D. Sharp, and E. G. Shelley, Geophys. Res. Lett. **4**, 403 (1977).

[2] D. Smith and N. G. Adams, Topics in Current Chemistry, Elementary Plasma Reactions of Environmental Interest 89 (1980).

[3] M. R. Torr, J. C. G. Walker, and D. G. Torr, J. Geophys. Res. **79**, 5267 (1974).

[4] M. R. Torr and D. G. Torr, Geophys. Res. Lett. **6**, 700 (1979).

[5] K. A. Smith, Measurement of Electron Loss Cross Sections for 0.25 - 5 keV Hydrogen Atoms in Atmospheric Gases, Ph. D. Thesis, Rice University 1976 (unpublished).

[6] D. A. Schafer, Differential Cross Sections for Neutral-Neutral and Charge-Transfer Collisions, M. A. Thesis, Rice University 1985 (unpublished).

[7] X. Li, Y. L. Huang, G. D. Flesch, and C. Y. Ng, J. Chem. Phys. **106** (4), 1373 (1997).

[8] R. D. Rundel, D. E. Nitz, K. A. Smith, M. W. Geis, and R. F. Stebbings, Phys Rev A **19** (1), 33 (1979)

[9] R. S. Gao, P. S. Gibner, J. H. Newman, K. A. Smith, and R. F. Stebbings, Rev. Sci. Instrum. **55** (11), 1756 (1984).

[10] L. K. Johnson, R. S. Gao, C. L. Hakes, K. A. Smith, and R. F Stebbings, Phys Rev A **40** (9), 4920 (1989).

[11] R. S. Gao, L. K. Johnson, D. A. Schafer, J. H. Newman, K. A. Smith, and R. F. Stebbins, Phys Rev A **38** (6), 2789 (1988).

[12] H. C. Straub, Absolute Partial Cross Sections for Electron-Impact Ionization of Ar, H_2, N_2, O_2, and CO_2 from Threshold to 1000 eV, Ph. D. Thesis, Rice University 1996 (unpublished).

[13] B. R. Turner, J. A. Rutherford, and D. M. J. Compton, J. Chem. Phys. **48**, 1602 (1968).

[14] T. F. Moran and J. B. Wilcox, J. Chem. Phys. **69** (4), 1397 (1978).

[15] G. J. Smith, Low Energy Elastic Scattering of O-Atoms by Atmospheric Species, Ph. D. Thesis, Rice University 1992 (unpublished).

[16] W. L. Williams and F. M. Goldberg, Metastable and Ground State Electron Loss Cross Sections for 2 - 6 keV Helium Atoms in Helium, Electronic and Atomic Collisions Abstracts, Vol. 2, 1087 (1971).

[17] R. S. Gao, Absolute Differential Cross Sections for Small-angle Charge-Transfer Collisions at keV Energies, Ph. D. Thesis, Rice University 1987 (unpublished).

[18] G. J. Smith, Absolute Differential Cross Sections for Electron Capture and Loss by keV Hydrogen Atoms, M. A. Thesis, Rice University 1990 (unpublished).

[19] R. S. Gao, G. J. Smith, K. A. Smith, unpublished

[20] R. F. Stebbings, B. R. Turner, and J. A. Rutherford, J. Geophysical Research 71 (3), 771 (1966).

IMAGE EVALUATION
TEST TARGET (QA-3)

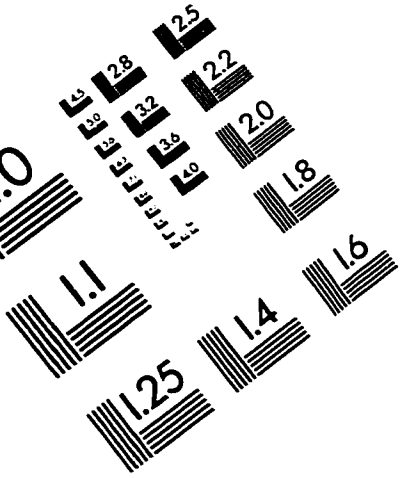

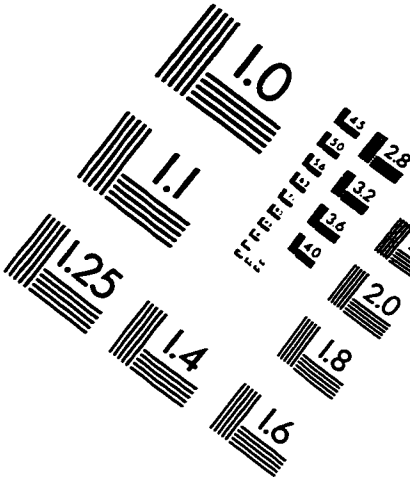

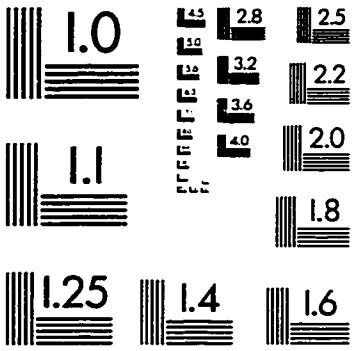

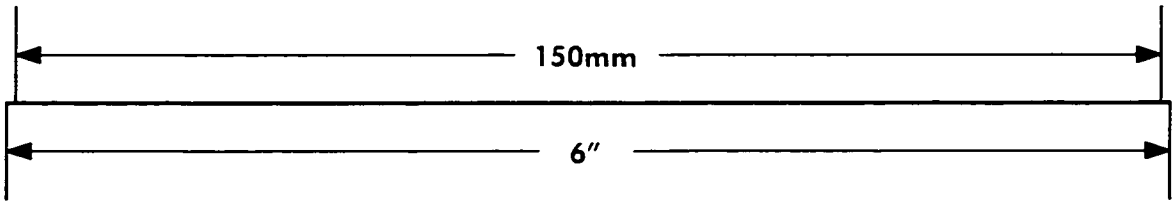

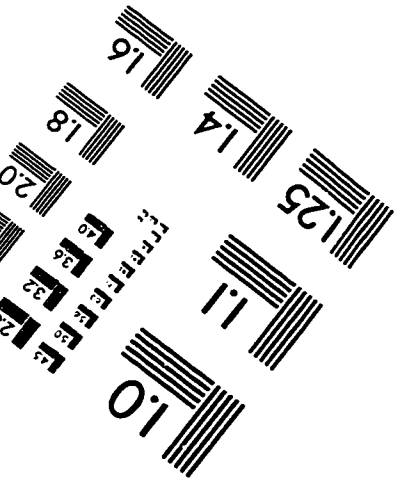

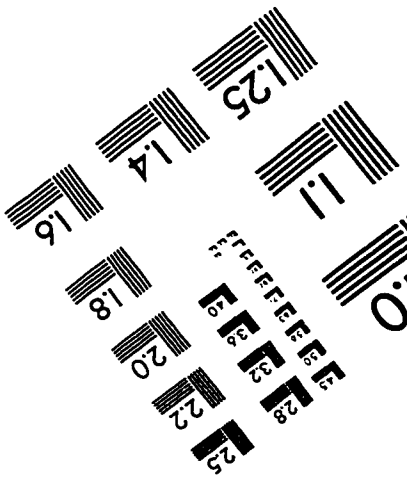

APPLIED IMAGE, Inc
1653 East Main Street
Rochester, NY 14609 USA
Phone: 716/482-0300
Fax: 716/288-5989